

Effect of Micro-Particle Additions on Frictional Energy Dissipation and Strength of
Concrete

Angela Madeo

Thesis submitted to the faculty of the Virginia Polytechnic Institute and State University
in partial fulfillment of the requirements for the degree of

Master of Science
In
Engineering Mechanics

Professor Norman E. Dowling, Chair
Associate Professor Scott Case
Professor Francesco dell'Isola
Associate Professor Scott Hendricks

February 8, 2006
Blacksburg, VA

Keywords: Concrete, frictional sliding, fillers, energy dissipation.

Effect of Micro-Particles Addition on Frictional Energy Dissipation and Strength of Concrete

Angela Madeo

ABSTRACT

This thesis is divided in two parts. The first part is devoted to the micro-macro modeling of the behavior of concrete under cyclic loading. Correlations between microscopic (frictional sliding of mesocracks) and macroscopic (energy dissipation) properties are investigated. The second part focuses on the description of a series of uniaxial cyclic tests on concrete and concrete-like materials performed at the "Rocks Mechanics Laboratory" of Virginia Polytechnic Institute and State University, Virginia, USA. Data deriving from these experiments are analyzed on the basis of the micro-macro identification theory. Interesting previsions on the real mechanical behavior of concrete can be found by means of the aforementioned theory and are presented in the last part of the thesis.

Acknowledgments

All the experiments presented in this thesis have been run in the "Rock Mechanics Laboratory" of Virginia Polytechnic Institute and State University. It is for this reason that special thanks go to the lab head, Professor Mario Karfakis, for his help with the testing apparatus. I must express sincere gratitude to Professor Norman E. Dowling for his precious help with the test preparation and development. I feel extremely grateful to him for the knowledge on mechanics of materials he transmitted to me during the time I spent at Virginia Tech and for the support he gave to my studies. Particular gratitude also goes to the Mechanical Behavior of Materials Lab head, Robert Simonds, for the irreplaceable technical help he gave me in the experimental setup and development and in setting up all the photographs presented in this thesis. Thank you also to the ESM Shop which provided the safety shields used during the tests, which worked efficiently, and for the creation of the particular plates needed to run the tests on oversized specimens. I also feel in debt to Professors Francesco dell'Isola and Giulio Sciarra from Università di Roma "La Sapienza" for their help on the theoretical part of my thesis. Last, but not least, I am deeply grateful to all the people who were close to me during my course of study and helped me reaching my objectives. Thank you to my parents, my brothers, and all the other people who feel close to me.

Contents

List of Figures	v
List of Tables	vii
1 Introduction	1
2 Theory and Background	3
3 Test Specimens and Materials	13
4 Test Apparatus and Procedure	18
4.1 Cyclic tests	19
4.2 Ramp failure tests	23
5 Test Results	24
5.1 Cyclic tests	24
5.2 Ramp failure tests	30
6 Analysis of results	33
6.1 Corrected energy dissipation	34
6.2 Micro-macro identification: evaluation of microscopic properties from macroscopic measurements	37
6.3 Possible correlation between the product ρd and the mechanical properties of the concrete-like materials.	60
7 Conclusions and Recommendations	70
A Energy dissipations	76
Bibliography	90

List of Figures

2.1	The i^{th} hysteresis loop for a typical concrete.	5
2.2	Triaxial cycling compression. From Pensée's PhD Thesis.	10
2.3	Evolution of the sliding parameter for two mesocracks families. From Pensée's PhD Thesis.	11
3.1	Typical cubic specimen of side 15 cm used in the tests run at Virginia Tech.	16
4.1	Sketch of the plates used for testing the concrete cubes of side 15 cm	19
4.2	Cyclic test settings.	20
4.3	Stress signal used for cyclic uniaxial tests at Virginia Tech. The stress on the y axis is a compressive stress.	21
4.4	The 4448 kN MTS Machine used for ramp failure tests. The clear plastic safety shield can be seen with a specimen in place behind it.	23
5.1	Typical hysteresis loop for unmodified concrete	25
5.2	Hysteresis loop detected for a CV0 specimen.	26
5.3	Hysteresis loop detected for a CG3 specimen.	26
5.4	Aluminum specimen tested to detect any possible friction phenomenon internal to the testing machine.	28
5.5	6061-T6 Al load vs. displacement curve	29
5.6	Stress level ($\sigma_{max}/\sigma_{at failure}$) versus fatigue life.	30
6.1	Graphical procedure to calculate a corrected energy dissipation.	35
6.2	Percent energy variation versus percentage of replacement for the modified concrete specimens	38
6.3	Cooling off behavior for CB specimens. Data from thermic tests run at the ISMA of Rome by order of "La Sapienza"	45
6.4	Cooling off behavior for CG specimens. Data from thermic tests run at the ISMA of Rome by order of "La Sapienza"	45
6.5	Cooling off behavior for CV specimens. Data from thermic tests run at the ISMA of Rome by order of "La Sapienza"	46
6.6	Cooling off behavior for CF specimens. Data from thermic tests run at the ISMA of Rome by order of "La Sapienza"	46

6.7	Macroscopic cracking for a CV0 specimen after few loading cycles	49
6.8	Variation of the product ρd with the percentage of replacement for each type of filler.	50
6.9	Frictional sliding of a crack in a CB3 specimen.	50
6.10	Frictional sliding of a crack in a CB7 specimen.	51
6.11	Frictional sliding of a crack in a CB0 specimen.	52
6.12	Frictional sliding of a crack in a CG3 specimen.	53
6.13	Frictional sliding of a crack in a CG7 specimen.	54
6.14	Frictional sliding of a crack in a CG0 specimen.	55
6.15	Frictional sliding of a crack in a CV3 and CF3 specimen.	56
6.16	Frictional sliding of a crack in a CV7 and CF7 specimen.	57
6.17	Frictional sliding of a crack in a CV0 and CF0 specimen.	58
6.18	Stresses at failure for all the percentages of replacement of the various fillers. Data from tests run at Virginia Tech.	61
6.19	Percent variation of the average energy dissipation of each specimen compared to the CSF energy variation. Data comes from cyclic tests run at Virginia Tech.	67
6.20	Percent variation of the product ρd as calculated from the coupling between the micro-macro frictional theory and the energy dissipation measures from cyclic tests.	67
6.21	Qualitative variation of the crack density d with respect to the CSF one. Data from thermic tests run at Università di Roma "La Sapienza".	68
6.22	Qualitative variation of the friction coefficient ρ for the various specimens with respect to the CSF one. This qualitative estimate has been made on the basis of the calculated values of the product ρd (see Fig. 6.20) and of the predicted crack density estimated from thermic analysis (see Fig. 6.21) . . .	68
6.23	Qualitative prediction of the stress at failure variation on the basis of the qualitative variations of ρ and d given in Fig. 6.21 and 6.22.	69
6.24	Actual stress at failure variation from measures deriving from ramp failure tests run at Virginia Tech.	69

List of Tables

3.1	Description of the fillers	14
3.2	Description of the specimens	15
3.3	Stress at failure from University of Rome "La Sapienza" ramp tests	17
4.1	Relative percentage stresses induced by a fixed stress range of 19.4 MPa	22
4.2	Load and stress ranges	22
5.1	Energy dissipations	27
5.2	Stress at failure from "Virginia Tech" ramp tests	31
5.3	Elastic moduli from Virginia Tech tests	32
6.1	Loads corresponding to P60	35
6.2	Corrected energy dissipations	36
6.3	Variation of the energy dissipation with respect to the CSF energy dissipation.	37
6.4	Calculated values of K1 for each material.	41
6.5	Estimated values for the product of the friction coefficient and the crack density	43
6.6	Estimated values for the product of the friction coefficient and the crack density	43
6.7	Crack density values for the various fillers and percentages of replacement relative to the CSF crack density dCSF	47

Chapter 1

Introduction

A set of compression tests on concrete specimens is presented in order to show how the presence of frictional mesocracks can affect the macroscopic behavior of the material once it is subjected to an external load. A crack is a cavity, one of whose dimensions is very small relative to the other two dimensions. For example, an elliptical crack can be regarded as an ellipsoidal cavity, the length of one of whose principal axes becomes very small in comparison with the length of the other two principal axes. When an external load is applied, the two superimposed faces of a crack start sliding on each other, generating a friction force that dissipates some of the energy applied to the specimen. The energy dissipated by friction represents a loss of energy of the system that cannot be recovered; it is for this reason that an hysteretic behavior for concrete specimens tested under cyclic load can be observed. If some microparticles are added to the concrete matrix in such a way that they can penetrate between the two faces of each crack, it can be expected that the energy dissipation due to friction phenomena changes according to the physical

properties of the microparticles themselves. In the particular case that will be presented, the concrete specimens used for testing differ from the common concrete specimens for the presence of some additives that can, in some way, change the frictional sliding behavior of the cracks under an external load. These additives, that will be called “fillers” for their ability of “filling” the voids of the concrete matrix, are of 4 types, and according to their intrinsic differences, they are expected to affect the energy dissipation in a different way. In order to measure the energy dissipation due to friction, the specimens have been tested in compressive cyclic loading and an estimate of the hysteresis loop area has been performed. As it will be shown later, the energy dissipation can be related, in some way, to the friction coefficient ρ between the two faces of each crack and to the crack density d of the specimen (d is a dimensionless parameter defined as the number of cracks per unit volume times the cube of the average radius of the crack). It is for this reason that, starting from the energy dissipation measured from the cyclic tests, an estimate of the product ρd can be performed. Furthermore, each specimen has been loaded until fracture in order to measure the compressive strength. In the remainder of this thesis, after a discussion of specimens, test methods and theories presented in literature, the results of tests conducted to determine the different energy loss due to different types of fillers are presented together with the connection between the measured energy dissipation and the mechanical properties of the materials.

Chapter 2

Theory and Background

Understanding and modeling of the inelastic behavior of microcracked materials have received considerable attention during the last twenty years. Continuum Damage Mechanics (CDM), based on the use of internal damage variables, constitutes undoubtedly the most appropriate framework for the analysis of the consequences of microcracking in engineering materials. When an external load is applied to a cracked material, the two superimposed faces of each crack start sliding on each other, generating a friction force that dissipates some of the energy provided from the external load itself. It is for this reason that a macroscopic hysteretic behavior of concrete under cyclic loading can be detected. It is clear that if the energy dissipation is mostly due to the frictional sliding of the internal microcracks (Pensée et al., 2002), a purely macroscopic approach is not sufficient to predict the mechanical behavior of a microcracked material (such as concrete). Since it allows us to relate the macroscopic properties to specific microstructural mechanisms, micromechanics may give a deeper insight of the behavior of a microcracked material subjected to a given

external load. In other words, micromechanics allows us to explain some macroscopic features, such as hysteresis under cycling loading, by means of microscopic phenomena, such as frictional sliding of microcracks (V. Pensée , D. Kondo, L. Dormieux, 2002). Consider, for sake of simplicity, a *uniaxial cyclic test* where a periodic load is applied to the specimen. In particular, the load, and then the uniaxial stress Σ , is assumed to vary in time following a sinusoidal law i.e.

$$\Sigma(t) = C + \Sigma_0 \sin(\omega t + \phi) \quad (2.1)$$

The uniaxial, sinusoidal, cyclic loading has been chosen because it will be used for the experiments which will be presented in the remainder of this thesis. For a generic loading cycle i , an energy dissipation due to the frictional sliding of mesocracks can be detected (see Fig. 2.1), and this energy can be measured as the area of the resulting hysteresis loop. Figure 2.1 shows a typical hysteresis loop for plain concrete; it refers to data obtained from experiments run at Virginia Tech as it will explained in the remainder of the thesis. Compression has been considered to have positive sign. Various micromechanical studies have been proposed by many authors in order to model the evolving damage due to progressive growth of distributed mesocracks and also to friction on cracks lips (see for instance Kachanov, 1982; Andrieux et al., 1986; Nemat-Nasser and Obata, 1988; Lee and Ju, 1991; Gambarotta and Lagomarsino, 1993; Pensée , Kondo, and Dormieux, 2002). In order to define a micromechanical model for a cracked brittle material like concrete, a Representative Element Volume (REV) must be defined. The REV, denoted by Ω , (with boundary $\delta\Omega$), consists in a volume composed of a solid matrix and multiple mesocracks with plane faces.

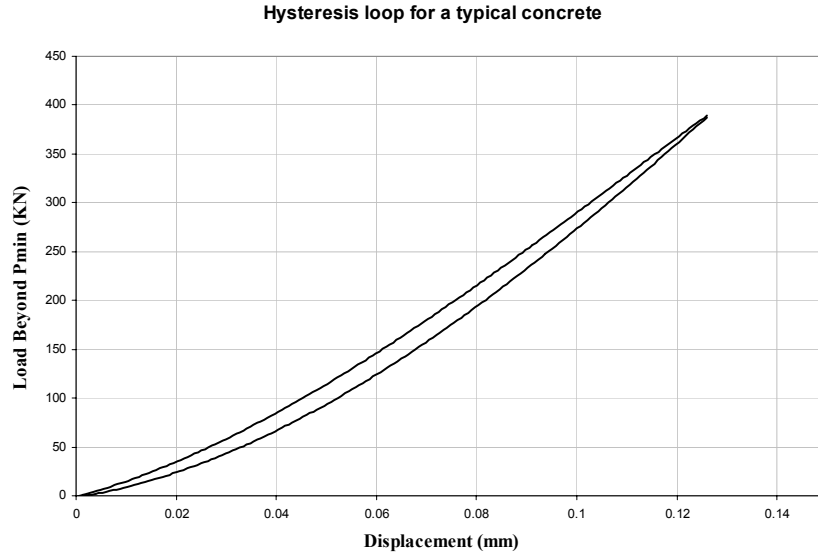


Figure 2.1: The i^{th} hysteresis loop for a typical concrete.

The solid matrix (undamaged material) is assumed to be isotropic and linear elastic with stiffness tensor \mathbf{C}^s (coefficients: E , λ , μ , ν). The domain occupied by a family of mesocracks (with unit normal \mathbf{n}) is denoted ω . Obviously ω is supposed to lie completely inside Ω . The displacement jump between the upper, ω^+ , and lower, ω^- , faces of the mesocracks is denoted $[\mathbf{u}]$. Mesocracks are assumed to have small size with respect to the REV dimension and to be closed in their initial state. The displacement discontinuity of any mesocracks family can be characterized by two variables: a scalar β (representing the crack opening) and the sliding vector $\boldsymbol{\gamma}$. These two parameters are defined as

$$\beta(\mathbf{n}) = N \int_{\omega^+} [u_n] da \quad (2.2)$$

$$\boldsymbol{\gamma}(\mathbf{n}) = N \int_{\omega^+} ([\mathbf{u}] - [u_n]\mathbf{n}) da \quad (2.3)$$

where N is the density (number per unit volume) of mesocracks. As it can be seen from Eq. (2.3), the magnitude of the sliding vector $|\boldsymbol{\gamma}|$ is a measure of the relative displacement of the two faces of a certain family of cracks that occupies a domain ω . It should be noted that both the scalar opening parameter β and the sliding vector $\boldsymbol{\gamma}$, as defined, depend on the normal \mathbf{n} of the corresponding generic family of penny-shaped cracks all having the same normal. As already seen, under compressive loading, some closed mesocracks may exhibit frictional sliding and generate complex macroscopic behavior. Some authors (see V. Pensée, D. Kondo, L. Dormieux, 2002) have developed a model based on CDM that is able to predict how microscopic frictional sliding can affect the macroscopic behavior of the material; this model will be briefly presented in the remainder of this paragraph. When mesocracks are closed ($\beta = 0$), non interacting and slide in the presence of friction, the macroscopic potential takes the form

$$W(\mathbf{E}, d, \boldsymbol{\gamma}) = \frac{1}{2} (\mathbf{E} - \mathbf{E}^{(2)}) : \mathbf{C}^s : (\mathbf{E} - \mathbf{E}^{(2)}) + \frac{K_1}{2d} \boldsymbol{\gamma} \cdot \boldsymbol{\gamma} \quad (2.4)$$

where

$$K_1 = \left(1 - \frac{\nu}{2}\right) K_0 \quad (2.5)$$

$$K_0 = \frac{3E}{16(1 - \nu^2)} \quad (2.6)$$

$$\mathbf{E}^{(2)} = \beta (\mathbf{n} \otimes \mathbf{n}) + \text{sym}(\boldsymbol{\gamma} \otimes \mathbf{n}) \quad (2.7)$$

$$d = Na^3 \quad (2.8)$$

with a average radius of the cracks in a REV, \mathbf{E} is the classic macroscopic strain tensor and $\mathbf{E}^{(2)}$ is the micro-strain tensor associated to the microcracks. The overall free energy, denoted by Ψ , can be written as the integral on the body of the potential W given in Eq.

(2.4). Assuming that the variation of the applied external macroscopic load occurs with a rate which is much slower than the rate of induced microdynamics phenomena, then one can accept the so called *Instantaneous Micro-Equilibrium Hypothesis*: At every instant, inside the REV, the micro-displacement field can be estimated to be equal to the field which is solution of the linear elastic problem formulated for the REV in which the external load is represented by the macro-stress field Σ considered as applied to the boundary of the REV.

As a consequence, under the quoted hypothesis, an expression for the sliding vector γ as a function of the macro stress tensor Σ can be deduced (see Pensée et al., 2002)

$$\gamma = \frac{d}{K_1} (\delta - \mathbf{n} \otimes \mathbf{n}) \cdot (\Sigma \cdot \mathbf{n}) \quad (2.9)$$

where \mathbf{n} is the unit vector normal to a given family of cracks and δ is the second order unit tensor. This expression for the sliding vector γ also lies on the non interacting mesocracks assumption. As explained before, the sliding vector γ , as defined in Eq. (2.3), represents a measure of the relative displacement between the two faces of a given family of cracks, so that if $\dot{\gamma}$ is the sliding rate, the volume energy dissipated over a cycle of period of time T can be written as

$$E_{vol}^{diss} = \int_0^T N \int_{\omega^+} \rho |F_n| |[\dot{\mathbf{u}}] - [\dot{u}_n] \mathbf{n}| da dt \quad (2.10)$$

where ρ is the dynamic friction coefficient and F_n is the surface specific friction force normal to the crack surface. When one can assume that ρ and $|F_n|$ are constant on all the cracks belonging to the considered family then the expression (2.10) reduces to

$$E_{vol}^{diss} = \rho \int_0^T |F_n| |\dot{\gamma}| dt := \rho \int_0^T |F_n| \sqrt{\dot{\gamma} \cdot \dot{\gamma}} dt \quad (2.11)$$

Equation (2.11) represents the energy dissipation per unit volume due to Coulomb's frictional sliding of mesocracks. Assuming that the magnitude of the normal friction force is

given by means of the following estimation

$$|F_n| = (\boldsymbol{\Sigma} \cdot \mathbf{n}) \cdot \mathbf{n} \quad (2.12)$$

and differentiating the expression (2.9) for γ with respect to time i.e.

$$\dot{\gamma} = \frac{d}{K_1} \left[\boldsymbol{\delta} \cdot (\dot{\boldsymbol{\Sigma}} \cdot \mathbf{n}) - (\mathbf{n} \otimes \mathbf{n}) \cdot (\dot{\boldsymbol{\Sigma}} \cdot \mathbf{n}) \right] \quad (2.13)$$

Eq. (2.11) gives

$$E_{vol}^{diss} = \rho \frac{d}{K_1} \int_0^T (\boldsymbol{\Sigma} \cdot \mathbf{n}) \cdot \mathbf{n} \sqrt{\left[\boldsymbol{\delta} \cdot (\dot{\boldsymbol{\Sigma}} \cdot \mathbf{n}) - (\mathbf{n} \otimes \mathbf{n}) \cdot (\dot{\boldsymbol{\Sigma}} \cdot \mathbf{n}) \right]^2} dt \quad (2.14)$$

If an uniaxial state of stress, as that one used in the tests run at the Rock Mechanics Laboratory of Virginia Tech, is considered, i.e.

$$\boldsymbol{\Sigma} = \Sigma_{33} \mathbf{e}_3 \otimes \mathbf{e}_3 := \sigma \mathbf{e}_3 \otimes \mathbf{e}_3 \quad (2.15)$$

and if the normal unit vector is written in terms of its component as

$$\mathbf{n} = n_i \mathbf{e}_i, \quad i = 1, 2, 3 \quad (2.16)$$

Eq. (2.13) gives

$$E_{vol}^{diss} = \rho \frac{d}{K_1} \int_0^T \sigma n_3^2 \sqrt{\dot{\sigma}^2 \left[n_3 \mathbf{e}_3 - n_3^2 (n_1 \mathbf{e}_1 + n_2 \mathbf{e}_2 + n_3 \mathbf{e}_3) \right]^2} dt \quad (2.17)$$

or

$$E_{vol}^{diss} = \rho \frac{d}{K_1} \int_0^T \sigma \dot{\sigma} n_3^3 \sqrt{[1 + n_3^2 (-2 + n_1^2 + n_2^2) + n_3^4]} dt \quad (2.18)$$

Considering this expression for E_{vol}^{diss} and considering that

$$n_1^2 + n_2^2 + n_3^2 = 1 \quad (2.19)$$

the energy dissipation over a period T becomes

$$E_{vol}^{diss}(\mathbf{n}) = \rho \frac{d}{K_1} \int_0^T \sigma \dot{\sigma} (1 - n_1^2 - n_2^2)^{3/2} \sqrt{(n_1^2 + n_2^2)} dt \quad (2.20)$$

This expression for the energy dissipation over a period T clearly depends on the unit normal \mathbf{n} , i.e. it depends on the particular family of mesocracks with normal \mathbf{n} considered. At this point if a *directionally uniform distribution of the mesocracks* is considered, a particular value for the energy E_{vol}^{diss} corresponding to an isotropic crack distribution can be found by integrating Eq. (2.20) over the unit sphere S , as follows

$$E_{vol}^{diss} = \int_S E_{vol}^{diss}(\mathbf{n}) d\mathbf{n} \quad (2.21)$$

or, considering Eq. (2.20)

$$E_{vol}^{diss} = \rho \frac{d}{K_1} \int_0^T \left[\sigma \dot{\sigma} \int_{-1}^1 dn_1 \int_{-\sqrt{1-n_1^2}}^{\sqrt{1-n_1^2}} (1 - n_1^2 - n_2^2)^{3/2} \sqrt{(n_1^2 + n_2^2)} dn_2 \right] dt \quad (2.22)$$

After a numerical integration over n_1 and n_2 the energy dissipation per unit volume over the i^{th} cycle of period T turns to be

$$E_{vol}^{diss} = \frac{0.61685 \rho d}{K_1} \int_0^T \sigma(t) \dot{\sigma}(t) dt \quad (2.23)$$

Where the uniaxial stress has an expression equivalent to the sine wave given by (2.1), i.e.

$$\sigma(t) = C + \sigma_0 \sin(\omega t + \phi) \quad (2.24)$$

The expression (2.23) for the energy dissipation together with the expression (2.24) will be used to analyze the results deriving from uniaxial cyclic tests on concrete performed at Virginia Tech. It must be noted that the expression (2.9) for the sliding vector γ deduced by Pensée et al., is valid only under the hypothesis of closed cracks ($\beta = 0$). It is for

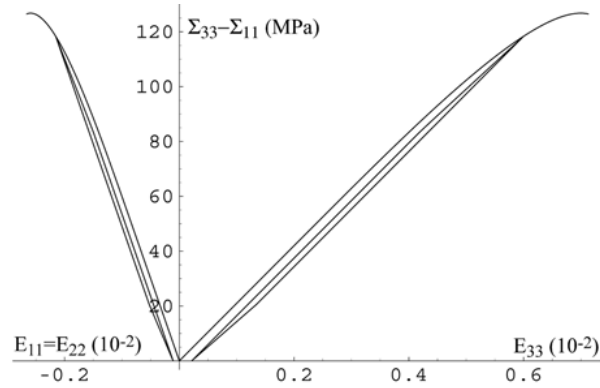


Figure 2.2: Triaxial cycling compression. From Pensée's PhD Thesis.

this reason that a pre-load must be applied to the specimen when expression (2.23) is used to estimate the energy dissipation over a cycle of period T . A more detailed discussion on the application of this theory to the experiments performed at Virginia Tech University will be presented in the remainder of this thesis. In the rest of this section, some results deduced by Pensée et al., are presented in order to show how the presence of the frictional mesocracks, damage evolution and plastic sliding can affect the energy dissipation of concrete subjected to an external cyclic load. Particular values for the parameters of the stiffness tensor \mathbf{C}^s , a crack density $d = 0.01$ and a friction coefficient $\rho = 0.6$ are chosen (see Pensée et al., 2002) and the stress-strain response shown in Fig. 2.2 is found. As it can be easily seen from Fig. (2.2), the model proposed by Pensée, Kondo and Dormieux is able to predict a macroscopic hysteretic behavior as a consequence of the presence of mesocracks in the material. The experiments that have been performed at Virginia Tech are uniaxial cyclic compression experiments, so that in this case $\Sigma_{11} = \Sigma_{22} = 0$, $\Sigma_{33} = \sigma$, (see definition given in (2.15)¹). Moreover the experimental conditions were established in order to be assured that (i) the

¹Numbers in parenthesis indicate equations.

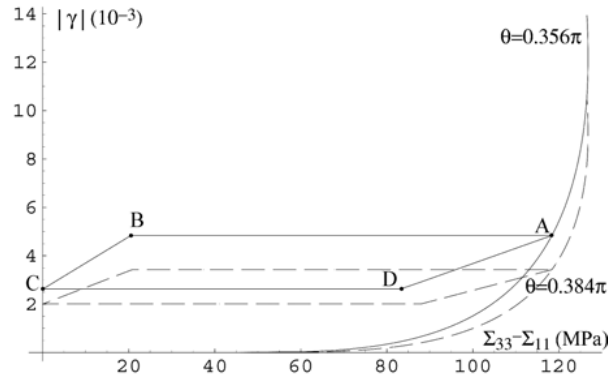


Figure 2.3: Evolution of the sliding parameter for two mesocracks families. From Pensée's PhD Thesis.

only relevant dissipation phenomenon was occurring because of sliding of crack faces and (ii) there was no occurrence of damage growth. On the basis of the theory presented by Pensée et al., 2002, it can be assumed that the macroscopic energy loss presented by a concrete specimen under compressive load is basically due to the frictional sliding of mesocracks in the material, particularly if it can be assumed that the mesocracks are closed ($\beta = 0$). As shown from Eq. (2.11), the macroscopic hysteretic behavior is correlated at mesoscale with the evolution of the sliding parameter γ associated to some closed cracks. It can be easily understood that the sliding vector γ depends on the macroscopic state of stress Σ induced to the specimen by an external load (see also Eq. (2.9)). Pensée et al., 2002, show the evolution of γ as a function of $\Sigma_{33} - \Sigma_{11}$ (simply of Σ_{33} for the uniaxial case) for two mesocracks families whose normal forms an angle ϑ with the loading axis; this evolution is shown in Fig. 2.3. Indeed, the loading-unloading and reloading of the material reveals the following successive steps (see Fig. 2.3):

- 1) Increase of the sliding parameter during loading (curve until A).
- 2) A step (AB) of sliding blocking which corresponds to the first part of unloading.

3) A backsliding step (BC) during which the sliding is mobilized in the opposite sense.

4) The reloading phase (CA) that confirms the origin of the macroscopic hysteretic loops.

On the basis of the theoretical structure presented up to now, a series of experimental tests has been performed in order to derive some information from the macroscopic energy dissipation measured from uniaxial cyclic compressive tests. Moreover, some micro-additives have been added to the cement paste in order to see if the frictional sliding is in some way affected by the presence of these micro-particles.

Chapter 3

Test Specimens and Materials

Concrete is a composite material that can be seen as a porous matrix in which pores of two different sizes can be located. In particular, families of pores of $\sim 10^{-3}\mu m$ and of $1-100\mu m$ can be detected. The second ones can be efficaciously modeled as families of mesocracks inside an undamaged matrix. These mesocracks have a great influence on the macroscopic mechanical properties of the concrete since they are expected to determine a decay in the average strength of the material. In fact, it is easy to understand that an undamaged matrix would have a better resistance to an external load than a porous matrix. On the basis of this analysis, together with the micro-macro theory previously presented, a set of concrete specimens with micro-additives has been prepared. Some additives, of a size such that they are able to penetrate inside the mesocracks, have been added to the cement paste resulting in the creation of new concrete-like materials. In order to see how the presence of these additives can affect the friction coefficient between the two faces of each crack together with the crack density inside the concrete matrix a series of experimental

Name of the additive	Size of the grains (μm)	Shape of the grains	Presence of film
Bianco Alago	1-40	Round	No
GS 4	1-35	Irregular	No
Valtochim	1-10	Irregular	Yes
Fillerchim	1-20	Irregular	Yes

Table 3.1: Description of the fillers

tests has been prepared. A testing procedure on these new materials has been set up and possible correlations between friction, crack density and mechanical properties of concrete are searched. It is clear that the friction coefficient depends on the physical properties of the additives, such as the shape and size of the grains and the roughness of the grains surface. It is for this reasons that additives of different size and shape have been used; moreover, some of the grains present a smooth film on their surface in order to lower the friction coefficient. In particular, 4 different types of additives have been chosen; each of them has an appropriate size to penetrate inside the mesocracks, but different physical properties. The main characteristics of these additives are shown in the table below:

These additives will be called “fillers” for their ability of “filling” the mesocracks of the matrix. All these fillers are obtained from carbonate rocks (such as inert limestone) so that the principal constituent (almost 99%) is Calcium Carbonate (CaCO_3). It has been shown, up to now, that the different fillers are expected to change, in some way, the friction coefficient on the basis of their physical properties. Another parameter that can affect the friction coefficient is the quantity of filler added to the cement paste. In fact, it can be easily understood that if the quantity of filler is irrelevant, the friction coefficient remains almost unvaried. On the other hand, if the quantity of filler added is higher than the quantity needed to fill all the voids, a certain amount of free additive remains in the cement paste,

Name of the specimen	Filler used for replacement	% of replacement
CSF	-	0
CB3	Bianco Alago	3
CB7	Bianco Alago	7
CB0	Bianco Alago	10
CG3	GS 4	3
CG7	GS 4	7
CG0	GS 4	10
CV3	Valtochim	3
CV7	Valtochim	7
CV0	Valtochim	10
CF3	Fillerchim	3
CF7	Fillerchim	7
CF0	Fillerchim	10

Table 3.2: Description of the specimens

affecting the normal chemical reactions and resulting in a variation of the overall mechanical properties of concrete. It is for this reason that an “optimal” quantity of additive must be found. In order to do so, specimens with different percentage of replacement have been created. More particularly, for each type of filler, a certain percentage in weight of the cement powder has been replaced with the same percentage in weight of filler. In the particular case in study, percentages of replacement of 3%, 7% and 10% have been chosen, resulting in the creation of 3 different specimens for each type of filler. Since the fillers used for this experiment are of 4 types (see Table 3.1), 12 different concrete + additive specimens have been prepared. Moreover, in order to compare the mechanical properties of the modified concrete with those of the normal concrete, an extra specimen of normal concrete has been added to the set, so that the total number of different specimens is 13. Table 3.2 lists all the different types of specimens used in the experiment.

In order to set a more accurate experiment, two specimens of each type have been



Figure 3.1: Typical cubic specimen of side 15 cm used in the tests run at Virginia Tech.

prepared, so that the final number of specimens tested is 26. The shape of the specimens is *cubic* and the side of the cube is 15 cm; a typical specimen is shown in Fig. (3.1). The shape and size chosen are those currently in use in Europe for concrete testing. In fact, the set of specimens previously described has been prepared by order of the Laboratorio di Strutture e Materiali Intelligenti, Università di Roma “La Sapienza”, Italy; they have then been sent to Virginia Polytechnic Institute and State University, Virginia, USA, in order to be tested under cyclic loading. It is worth to mention that a compression ramp test has already been performed on the same set of specimens at the Università di Roma. The test run at “La Sapienza” is simply a ramp test (the specimen is loaded until its failure) so that the energy dissipation during cyclic loading cannot be measured; in any case, some useful information on the mechanical properties of the materials can still be found. The most important information is undoubtedly given by the average values for the strength at

Specimen type	Avg. stress at failure σ_f (MPa)
CSF	32.4
CB3	33.1
CB7	33.2
CB0	27.8
CG3	43.2
CG7	29.6
CG0	29.7
CV3	31.7
CV7	26.8
CV0	24.2
CF3	32.9
CF7	35.1
CF0	32.3

Table 3.3: Stress at failure from University of Rome "La Sapienza" ramp tests

failure of each specimen. These values are listed in Table 3.3.

Each value of σ_f in Table 3.3 is obtained as an average of 2 values deriving from tests on 2 different specimens of the same type. Additional information and comparison of these results with those obtained from the cyclic test will be given in the reminder of this thesis.

Chapter 4

Test Apparatus and Procedure

All specimens were tested following two different procedures. As a first step, each specimen was tested under cyclic loading on a closed loop, servohydraulic testing machine made by MTS Systems Inc. This machine had a 500 kN capacity, with the load cell calibrated to 444.8 kN. After the cyclic test was performed, a ramp test to failure was run on each specimen on a 4448 kN MTS Machine. The ramp test was run on a different machine because the load at failure for the cubic concrete specimens (almost 800 kN) exceeded the capacity of the machine used for cycling. Both the cyclic and the ramp tests had spherical-seat grips in order to assure axial load without bending. The loading plates used were specifically made for the present experiment because the specimen dimensions exceeded the original plates dimensions; a sketch of the plates with their dimensions is shown in Fig. (4.1). These new plates had a recessed area to fit the 8 inch diameter original plates, and to assure centering. Round concentric marks were scribed on both loading plates in order to aid in positioning the specimens on center.

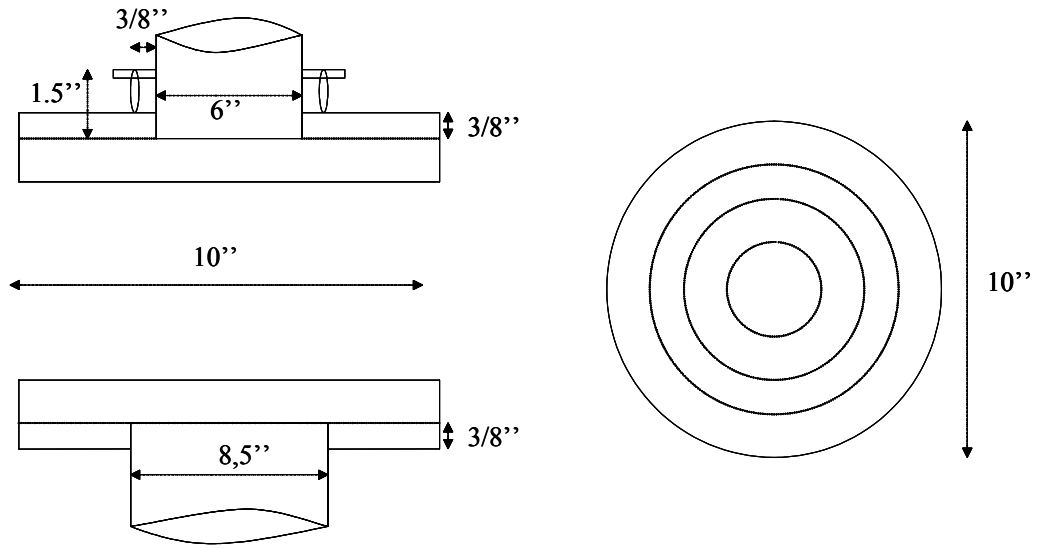


Figure 4.1: Sketch of the plates used for testing the concrete cubes of side 15 cm

4.1 Cyclic tests

Strains were measured using an extensometer attached to the lower loading plate with a magnetic mount and configured to measure the relative displacement between the upper and the lower loading plates (see Fig. 4.2). Hence, the extensometer measured strains over the full 15 cm length of the specimen. An extra set of strain measures, used simply for a comparison with the extensometer data, was collected by monitoring the testing machine motion. This motion was measured by an LDTV (Linear Variable Differential Transformer); this device is able to sense the motion of the hydraulic actuator, so these measurements also include the deflection in the grips, load cell, crosshead and posts of the testing machines. The displacement measured by the LDTV was found to be almost doubled with respect to the one measured by the extensometer. This means that the plates deflected, in some way, during the experiment. In any case, considering the deflection in

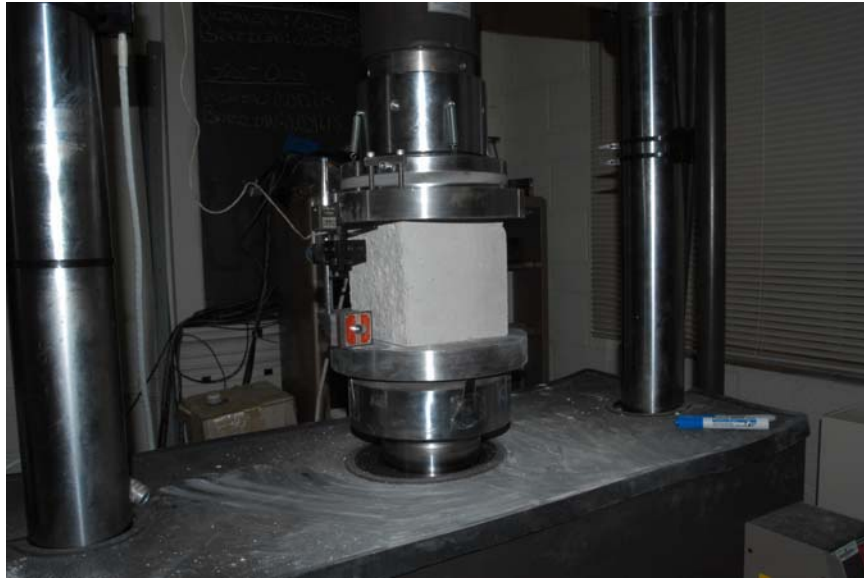


Figure 4.2: Cyclic test settings.

the plates to be elastic (which is in fact the case for the particular load applied), the overall energy dissipation measured can be related uniquely to the concrete specimens. Stress was controlled and a fixed frequency of 0.2 Hz was chosen for all the tests. The stress signal was imposed to be a sine wave like that one considered in Eq. (2.24). More particularly, the sine wave used for loading assumes the following form

$$\sigma(t) = \left(\sigma_{\min} + \frac{\Delta\sigma}{2} \right) + \frac{\Delta\sigma}{2} \sin \left(-\frac{\pi}{2} + \frac{2\pi}{5}t \right) \quad (4.1)$$

where the values for σ_{\min} and $\Delta\sigma$ are given in Table 4.2. The sinusoidal stress given from Eq. (4.1) is shown in Fig. 4.3 for the particular case of the tests run at Virginia Tech. A number of 100 cycles was chosen for each test. An MTS software was used to collect data. The peak stress was chosen in order to reach approximately the 60% of the unmodified concrete stress at failure (60% of CSF σ_f) In particular, a peak stress of 19.42 MPa was chosen.

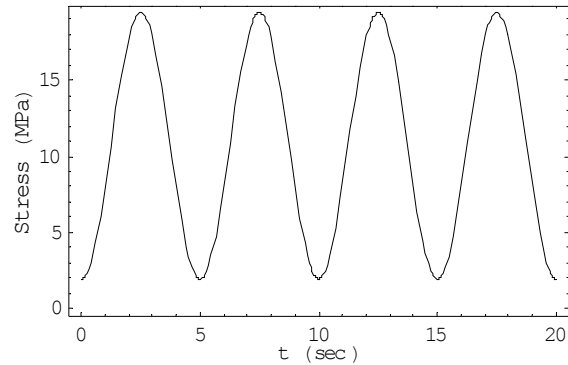


Figure 4.3: Stress signal used for cyclic uniaxial tests at Virginia Tech. The stress on the y axis is a compressive stress.

Since the average σ_f differs from a specimen type to another, so the stress range chosen represents a different relative percentage of σ_f for each specimen. In other words, 19.42 MPa represents a different percentage of the stress at failure σ_f for each different specimen; these relative percentages are shown in Table 4.1 and are referred to the values of σ_f shown in Table 3.3. This different relative stress ranges will affect in some way the behavior of each specimen during the test and their influence must then be taken into account in a further data analysis. Considering the shape and size of the specimens, an applied peak stress of 19.42 MPa corresponds to an applied peak load of approximately 437 kN. For particular theoretical needs due to the necessity of having closed cracks ($\beta = 0$), each specimen was manually preloaded until it reached a load of 43.7 kN (10% of the load peak), and then the load was cycled between this minimum and a maximum of 437 kN. The resulting load range is then approximately equal to 393.3 kN. Moreover, the nonzero minimum load was also convenient for testing, as it avoided loss of contact with the specimen at zero load, which would be expected to cause extraneous motions that would affect the strain data. The load and stress ranges used are clearly summarized in the table below

Specimen type	% of σ_f
CSF	60.0
CB3	58.6
CB7	58.5
CB0	69.9
CG3	45.0
CG7	65.7
CG0	65.5
CV3	61.3
CV7	72.5
CV0	80.3
CF3	59.1
CF7	55.3
CF0	60.1

Table 4.1: Relative percentage stresses induced by a fixed stress range of 19.4 MPa

σ_{\min} (MPa)	σ_{\max} (MPa)	P_{\min} (kN)	P_{\max} (kN)
1.942	19.42	43.7	437
$\Delta\sigma$ (MPa)		ΔP (kN)	
17.48		393.3	

Table 4.2: Load and stress ranges



Figure 4.4: The 4448 kN MTS Machine used for ramp failure tests. The clear plastic safety shield can be seen with a specimen in place behind it.

4.2 Ramp failure tests

After being tested in cyclic compressive loading, all the specimens were tested with a classical ramp test. In order to run this test on the same set of specimens used for cycling, it was assumed that the cyclic test did not affect the mechanical resistance. It will be explained later that this hypothesis has been found to be sensible. All ramp tests were run on the 4448 kN MTS Machine (see Fig. 4.4). Testing machine motion was controlled during the ramp failure tests. An MTS software was used to collect data. The failure load was measured for each specimen.

Chapter 5

Test Results

5.1 Cyclic tests

As a consequence of the cyclic loading, hysteresis loops for each specimen have been detected. As already discussed in the previous sections, the energy dissipation associated with each hysteresis loop is basically due to the frictional sliding of the mesocracks in the concrete matrix (see Pensée et al., 2002). A typical hysteresis loop from cyclic experiments run at Virginia Tech is shown in Fig. 5.1. As can be seen from this hysteresis loop, the initial load appears to be equal to zero and to reach the value 393.3 kN. This means (see Table 4.2) that the graphic shown refers to load ranges instead that to the actual applied load. Specifically, compressive loads are considered positive, and the load scale represents only the load beyond P_{min} , so that the quantity plotted is $(P - P_{min})$. The same convention is also followed for all other hysteresis loop plots shown later. As expected, different energy dissipations were found for concrete specimens modified with different fillers. More particularly, both higher (see Fig. 5.2) and lower (see Fig. 5.3) energy dissipations

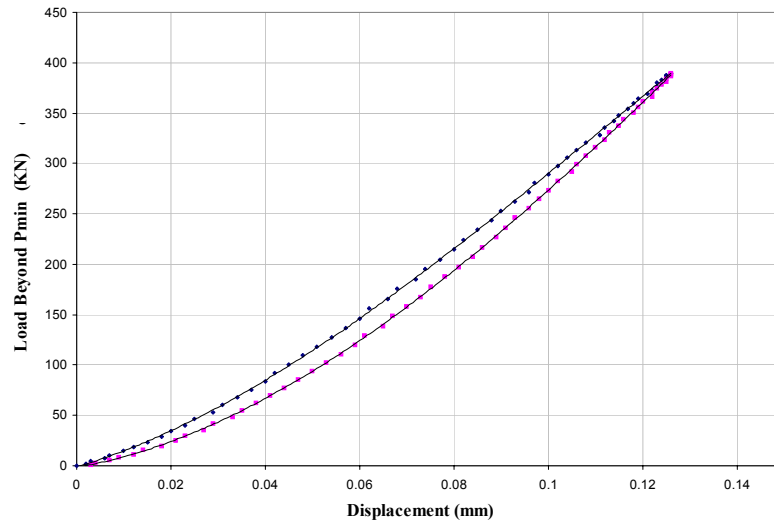


Figure 5.1: Typical hysteresis loop for unmodified concrete

were measured, corresponding to different fillers and percentage of replacement. It must be said that data corresponding to CG0 and CV0 specimens were found to be not consistent, since the scatter of the energy dissipations between the two specimen of each type was found to be very high. This phenomenon was explained as a likely error of the manufacturer in writing the name on the specimens. In fact simply changing a CG0 specimen with a CV0 one the values of the energy dissipations presented negligible scatters and the values of the stress at failure were found to be comparable to that one previously measured at "La Sapienza". Figure 5.1 shows the typical load-displacement behavior of an unmodified concrete specimen tested under cyclic loading. As known, the area between the upper and the lower curve represents the measured energy dissipation of the material. Energy dissipations for each specimen have been measured by means of a fixed procedure which will be discussed in the

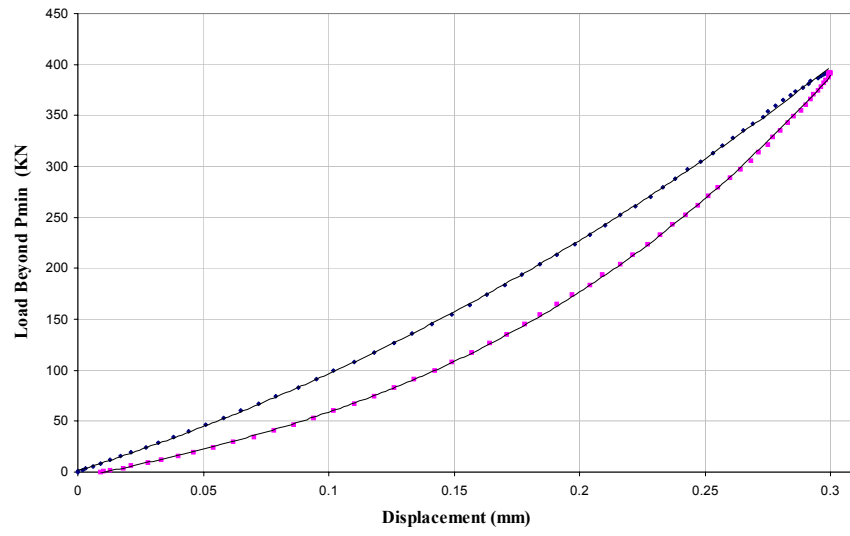


Figure 5.2: Hysteresis loop detected for a CV0 specimen.

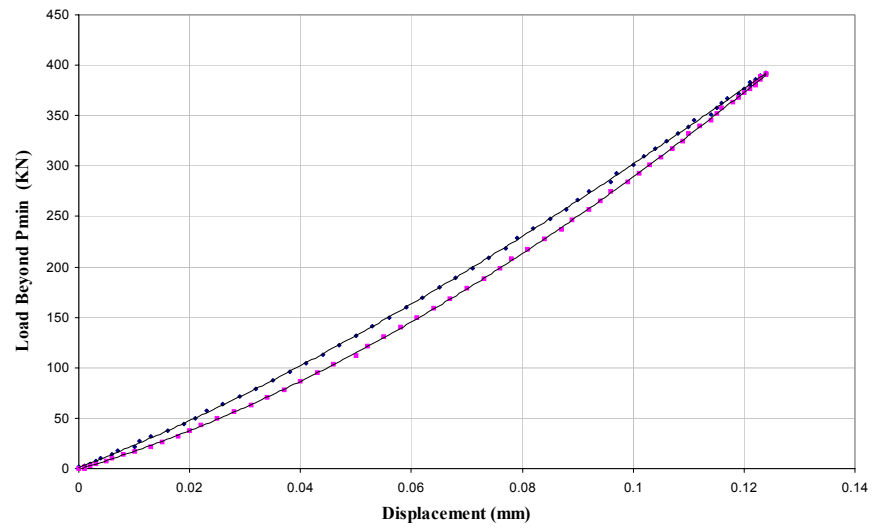


Figure 5.3: Hysteresis loop detected for a CG3 specimen.

Specimen	Average Energy dissipation (J)
CSF	2.0
CB3	2.4
CB7	2.2
CB0	2.9
CG3	1.8
CG7	3.3
CG0	2.8
CV3	2.4
CV7	2.5
CV0	9.2
CF3	2.0
CF7	2.6
CF0	4.5

Table 5.1: Energy dissipations

following and the obtained average value (calculated on 2 specimens) is shown in Table 5.1.

. The procedure used to measure the energy dissipation is the same for each specimen and can be summarized as follows

1) Chosen a specific cycle i approximately in the middle of the experiment, two 3^{rd} order polynomials have been fitted both on the loading and unloading data points (see Fig. 5.1).

2) The area under each curve (loading and unloading curve) has been calculated by mean of a simple definite integration.

3) The area under the lower curve has been subtracted from the area under the upper curve. The energies reported in Table 5.1 are relative to a cycle in the middle of the experiment (usually the 50^{th}) which can be assumed to represent the stable behavior of the material. In fact, before the 50^{th} cycle was chosen as representative cycle, other different cycles were analyzed, but the energy dissipations were found not to differ in a



Figure 5.4: Aluminum specimen tested to detect any possible friction phenomenon internal to the testing machine.

significant way from each other. In order to be sure that the measured hysteretic behavior was not due to hysteretic phenomena connected with the testing machine, a cyclic test on an aluminum specimen was run. A square cross section specimen of side 3.5 inches (88.9 mm) and height 6.0 inches (152.4 mm) of precipitation hardened aluminum alloy (probably 6061-T6), (see Fig. 5.4), was tested under the same load range used for the concrete specimens (see Table 4.2). The peak stress induced by this load is approximately equal to 55.3 MPa which is well below the yield stress of the aluminum (for failure stresses of various aluminum alloys, see Dowling, 1999, pg 120), so that a linear-elastic behavior of the specimen is expected in absence of internal hysteresis of the machine. A quasi linear elastic behavior was actually measured during the experiment (see Fig. 5.5), so it can be assumed that the energy dissipation measured from the concrete cyclic test is totally due to friction phenomena inside the cement paste. As can be seen from Fig. 5.5, a small hysteretic

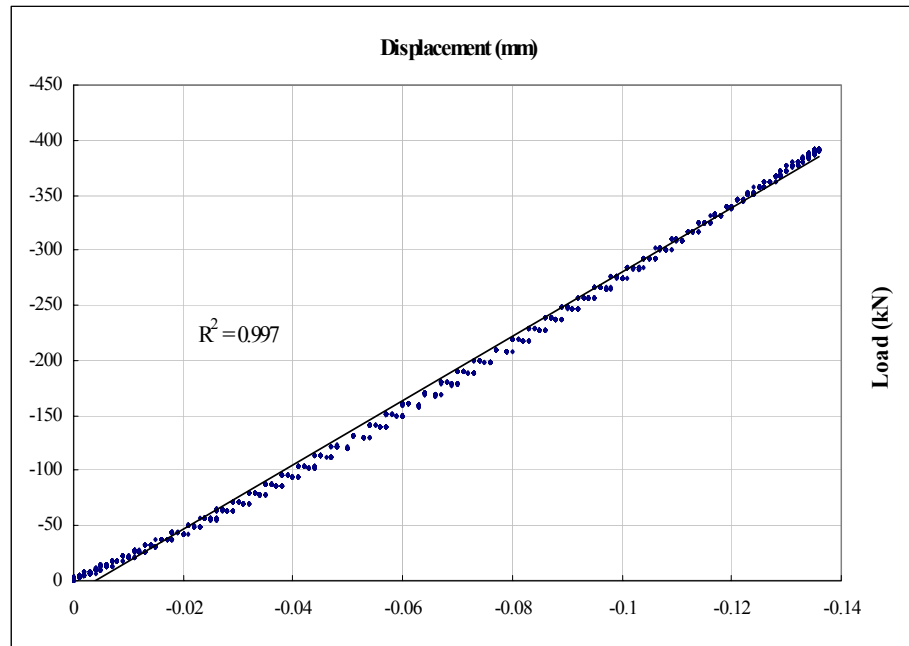


Figure 5.5: 6061-T6 Al load vs. displacement curve

behavior, probably due to friction internal to the machine, or between specimen and grips, can still be measured. The energy dissipation for the aluminum block was calculated to be almost equal to 0.7 J which almost 1/4 of the minimum energy dissipation calculated for concrete-like materials (see Tab. 5.1). However, since this dissipation is small compared to those measured from concrete specimens (see Fig. 5.1), it will be assumed that it is equal to zero. In other words, the energy dissipation measured from concrete specimens will be totally attributed to a real material behavior, rather than to some effects due to the test apparatus. An analysis of the results shown in this section will be given in the remainder of this thesis.

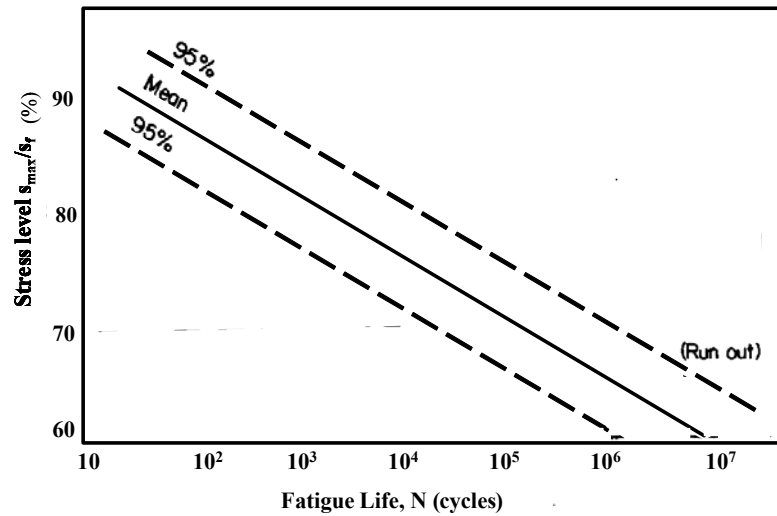


Figure 5.6: Stress level (sigma max/sigma at failure) versus fatigue life.

5.2 Ramp failure tests

As briefly explained before, each specimen tested under uniaxial cyclic load was finally tested with a ramp test in order to measure its final resistance. Assuming that the stress range applied to the specimen is 60% of the failure stress (see Table 4.1), it can be predicted that failure under these conditions happens around $10^6 - 10^7$ cycles (see Bennet, 1980). Various fatigue experimental results on plain concrete can in fact be found in literature so that the number of cycle to failure can be estimated (see Fig. 5.6). Since the cycling was limited to 100 cycles it can be assumed that the cycling process did not significantly affect the mechanical properties of the specimens. If this hypothesis is sensible, the failure strength of each specimen is expected to be comparable to that one measured in the University of Rome ramp tests. The average failure strengths measured at the University

Specimen	Average stress at Failure σ_f (MPa)
CSF	34.6
CB3	32.0
CB7	34.2
CB0	32.6
CG3	40.0
CG7	29.8
CG0	30.7
CV3	32.1
CV7	28.6
CV0	24.3
CF3	33.1
CF7	34.5
CF0	26.4

Table 5.2: Stress at failure from "Virginia Tech" ramp tests

of Rome are shown in Table 3.3. It can be immediately noticed that the average stresses at failure shown in Table 5.2 are reasonably consistent with those shown in Table 3.3. Therefore, the assumption according to which 100 cycles at 60% of σ_f do not considerably affect the mechanical behavior of the concrete can be considered sensible, except perhaps for the CF0 specimens. Further discussions and analysis of the stresses at failure for the various specimens will be given in the next section. Finally, the elastic modulus has been calculated (as an average value over the entire nonlinear curve) for each specimen referring to data collected during the cyclic tests; the values for the average elastic moduli are given in Table 5.3.

Specimen	Average Elastic Modulus E (GPa)
CSF	23.3
CB3	19.7
CB7	19.5
CB0	17.5
CG3	23.0
CG7	18.0
CG0	18.2
CV3	19.8
CV7	19.3
CV0	11.4
CF3	19.0
CF7	23.0
CF0	16.0

Table 5.3: Elastic moduli from Virginia Tech tests

Chapter 6

Analysis of results

In this section an analysis of the macroscopic energy dissipations shown in Table 5.1 will be performed and a connection with the microscopic properties of each material will be attempted on the basis of the theory presented in the theory section. Moreover, a possible connection between the energy dissipation due to friction phenomena and the overall mechanical properties of the material will be searched. It must be noted that, in order to compare the energy dissipations of different materials, each of them should have been tested at the same percentage of its failure strength. In fact, it is intuitive that if a specimen is tested with a stress close to its failure stress, the energy dissipation is expected to be higher than if the specimen was tested with a lower stress level. It has been seen (Tab. 4.1) that each specimen has been actually tested at a different relative percentage stress, so that a procedure which can get all the tests comparable is needed.

6.1 Corrected energy dissipation

A corrected energy dissipation for each material has been calculated by mean of the following procedure:

1) The load P_{60} approximately corresponding to the 60% of the failure stress σ_f has been calculated for each specimen. The average failure stresses calculated from Virginia Tech ramp tests have been used as reference failure stresses (see Table 5.2). Different P_{60} corresponding to different specimens are shown in Table 6.1.

2) The load vs. displacement curve branch corresponding to the loading path (blue curve in Fig. 6.1) has been drawn until reaching the load P_{60} corresponding to 60% of σ_f (point A).

3) The corresponding displacement d_{60} has been calculated (see Fig. 6.1)

4) A polynomial fitting a part of the unloading data points and point A has been drawn (pink curve).

5) The area of the resulting hysteresis loop has been calculated. This area represents the corrected energy dissipation corresponding to an applied load equal to P_{60} . It must be noted that the procedure shown in Fig. 6.1 is valid for the case in which $P_{60} \leq P_{\max}$, where P_{\max} is the maximum load applied. When $P_{60} > P_{\max}$ the same procedure has been applied assuming that the third order polynomial fitting the loading data can be prolonged until reaching P_{60} .

The corrected average energy dissipations obtained by mean of the empirical procedure described above are shown in Table 6.2. In order to easily compare the various corrected energy dissipations to the one corresponding to the unmodified concrete (CSF),

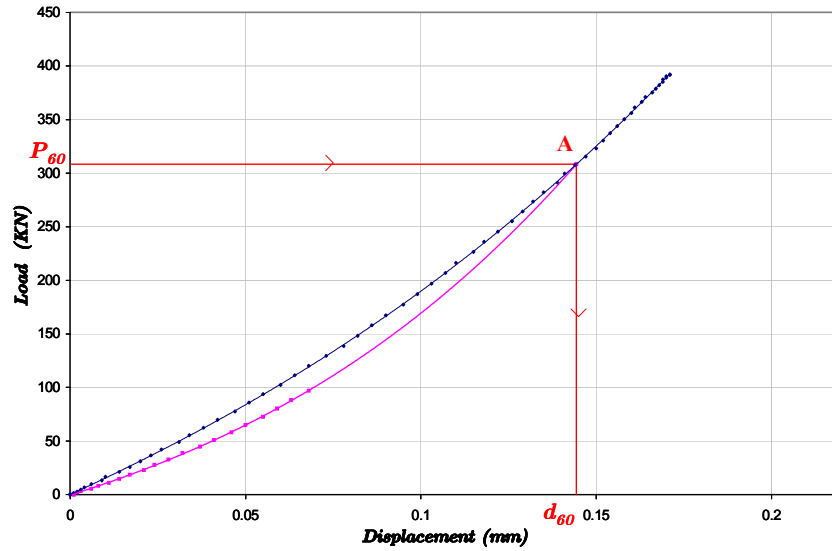


Figure 6.1: Graphical procedure to calculate a corrected energy dissipation.

Specimen	P60 (kN)	Actual Load (kN)
CSF	423.1	393.3
CB3	388.7	393.3
CB7	417.7	393.3
CB0	397.1	393.3
CG3	496.3	393.3
CG7	358.5	393.3
CG0	370.9	393.3
CV3	389.7	393.3
CV7	341.9	393.3
CV0	284.3	393.3
CF3	402.6	393.3
CF7	422.6	393.3
CF0	313.4	393.3

Table 6.1: Loads corresponding to P60

Specimen	Avg. En. Diss. (J)	Avg. Corrected En. Diss. (J)
CSF	2.0	2.1
CB3	2.4	2.4
CB7	2.2	2.2
CB0	2.9	2.9
CG3	1.8	2.3
CG7	3.3	3.1
CG0	2.8	2.6
CV3	2.4	2.4
CV7	2.5	2.2
CV0	9.2	6.3
CF3	2.0	2.0
CF7	1.7	1.8
CF0	4.5	3.6

Table 6.2: Corrected energy dissipations

percentage variations (ΔE) are shown in the table below. It must be kept in mind that ΔE represents the variation of the energy dissipation of a given material with respect to the energy dissipation of the unmodified concrete. As it will be clarified in the next section, the measurement of the macroscopic energy dissipation is not sufficient to describe the microscopic behavior of the material. In fact, other quantities like the material constant K_1 and the applied stress $\sigma(t)$ must be known in order to perform a micro-macro identification (see Eq. (2.23)). So, the connection between the energy dissipation and the microscopic phenomena inside the concrete matrix is not intuitive and an appropriate description of these phenomena needs a deep theoretical analysis. This analysis will be performed in the next section. In any case, the variation of ΔE versus the percentage of replacement is reported in Fig. 6.2 in order to clarify that the variation in the energy dissipation depends not only on the type of filler, but also on the percentage of replacement. This analysis of the properties of the modified concrete as a function of the filler percentage of replacement will be widely

Specimen	% ΔE (J)
CSF	reference
CB3	+14.8
CB7	+7.1
CB0	+40.5
CG3	+8.1
CG7	+46.2
CG0	+23.3
CV3	+13.8
CV7	+5.7
CV0	+199.5
CF3	-1.4
CF7	-15.0
CF0	+71.9

Table 6.3: Variation of the energy dissipation with respect to the CSF energy dissipation.

used in the reminder of this thesis, in order to find if there is some "optimal" percentage of replacement, such that the mechanical properties of concrete can be improved.

6.2 Micro-macro identification: evaluation of microscopic properties from macroscopic measurements

A micro-macro identification is a procedure that to creates a theoretical connection between microscopic and macroscopic properties. As has already explained before (see Pensée et al., 2002), the macroscopic energy dissipation of concrete due to the application of an external cyclic load can be connected, in some way, with the frictional sliding of mesocracks inside the material. At this point a micro-macro identification will be attempted on the basis of the theoretical structure presented before. As has been previously shown, macroscopic measurements of the energy dissipations under cyclic loading have been

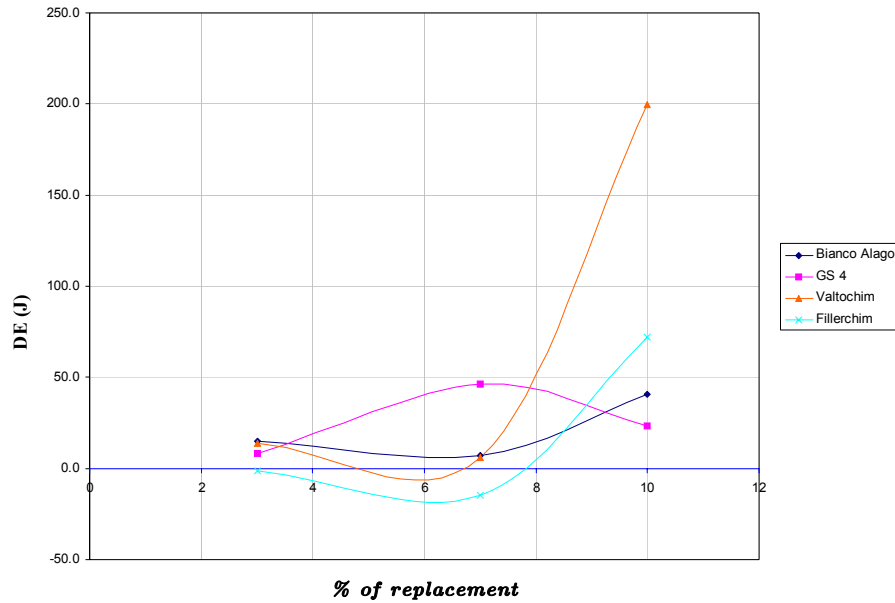


Figure 6.2: Percent energy variation versus percentage of replacement for the modified concrete specimens

performed for different concrete-like materials (see Table 6.2). It can be easily understood that if the energy dissipation E_{vol}^{diss} in Eq. (2.23) is assumed to be known from experimental measurements, the only unknowns in Eq. (2.23) remain the friction coefficient ρ and the crack density d . In fact, the stress function $\sigma(t)$ is known and given by Eq. (4.1) and so is the stress rate $\dot{\sigma}(t)$. Moreover, the constant K_1 defined by Eq. (2.5) is uniquely determined from the Poisson's coefficient ν and the Young's modulus E of the material (values are given in table 5.3). At this point the procedure used to calculate the quantity ρd is shown for the the unmodified concrete (CSF), while the values calculated for the other specimens are simply shown in Table 6.5. As a first step Eq. (2.23) is considered, i.e.

$$E_{vol}^{diss} = \frac{0.61685 \rho d}{K_1} \int_0^T \sigma(t) \dot{\sigma}(t) dt \quad (6.1)$$

It must be noticed that this expression for the specific volume energy dissipation has been deduced on the basis of some hypothesis needed to simplify the structure of the model presented by Pensée et al., 2002. The hypothesis used to get Eq. (6.1) are briefly recalled in the following together with their physical meaning.

1. *Instantaneous Micro-Equilibrium Hypothesis*, (see Eq. (2.9)): the variation of the applied external macroscopic load occurs with a rate which is much slower than the rate of induced microdynamics phenomena. At every instant, inside the REV, the micro-displacement field can be estimated to be equal to the field which is the solution of the linear elastic problem formulated for the REV in which the external load is represented by the macro-stress field Σ considered as applied to the boundary of the REV. This hypothesis can be considered sensible, at least in an approximate sense, in the special case of the cyclic tests run at Virginia Tech. In fact, the frequency of the sinusoidal stress function used in the aforementioned tests was set to be 0.2 Hz. This means that each complete stress cycle had the duration of 5 seconds and then the macroscopic stress took 2.5 seconds to get from 0 to the maximum value and 2.5 seconds to reach the zero again. This period of time has been estimated to be sufficiently large to let the Micro-Equilibrium Hypothesis holds.
2. *Non interacting mesocracks*. It was assumed that each crack slides without feeling the influence of the other mesocracks.
3. *Directionally uniform distribution of the mesocracks*, see Eq. (2.21). This hypothesis is clearly a simplification whose validity has to be checked. In fact, we are assuming that for each given direction the number of cracks pointing in that direction is always

the same. This will certainly not be the real case, but since a careful procedure has been set up for the preparation of the specimens, the hypothesis can still be considered sensible, even if as an approximation. In fact, particular attention was used during the mixing of the cement paste and during the fillers addition to assure uniform distributions. Moreover, the cement paste was put in the cubic mould very slowly and carefully.

4. *Absence of damage evolution* during the cycling. With this hypothesis we are assuming that the load is low enough to let the crack density d remain constant during the cyclic test. In this way, the product of the friction coefficient ρ and the crack density d can be considered to be constant over each cycle. This hypothesis can be considered sensible since the fatigue failure of a concrete specimen under a load whose stress range is set to be $\sim 60\%$ of the failure stress is expected to happen around $10^6 - 10^7$ cycles (see Fig. (5.6)). The cyclic tests run at Virginia Tech used a stress range of $\sim 60\%$ of the failure stress and the cyclic period was limited to 100 cycles, so that the material can be considered to be basically undamaged.

5. *Initially closed mesocracks*. We are assuming that the crack opening parameter β defined in Eq. (2.2) is equal to zero. This means that the two faces of each crack are assumed to be in contact before they start sliding on each other. In order to assure this contact, a pre-load of 43.7 kN has been applied to the specimen before the beginning of the cyclic test. This load has been assumed to be high enough to cause contact between the two faces of each crack, avoiding any pre-sliding.

Specimen	K_1 (MPa)
CSF	1.7
CB3	1.4
CB7	1.4
CB0	1.3
CG3	1.7
CG7	1.3
CG0	1.3
CV3	1.4
CV7	1.4
CV0	0.8
CF3	1.4
CF7	1.6
CF0	1.1

Table 6.4: Calculated values of K_1 for each material.

At this point, assuming that the Poisson's coefficient of all the specimens is $\nu = 0.3$ and that the Young's modulus for each material is given in Table 5.3, values of K_1 for each material can be calculated and they are shown in Table 6.4. Using the value of K_1 for CSF in Eq. (6.1) we get

$$E_{vol}^{diss} = 0.3716 \rho d \int_0^T \sigma(t) \dot{\sigma}(t) dt \quad (6.2)$$

Recalling that the test frequency was set to be 0.2 Hz (cycles per second) for every cyclic test, the resulting period T needed to finish one cycle is obviously 5 sec. So, the above equation for the particular test settings used at Virginia Tech turns to be

$$E_{vol}^{diss} = 0.3716 \rho d \int_0^5 \sigma(t) \dot{\sigma}(t) dt \quad (6.3)$$

where $\sigma(t)$ is given by Eq. (4.1). The integral in the previous equation can be calculated with a simple numerical integration so that the volume energy dissipation for CSF calculated

by mean of the frictional cracks theory turns to be

$$E_{vol}^{diss} = 8443\rho d \quad (6.4)$$

Considering that the specimen volume is 3.375×10^{-3} we finally get that the theoretical energy dissipation E^{diss} over a CSF specimen of the same shape and size of that one used for testing at Virginia Tech is

$$E^{diss} = 28.5\rho d \quad (6.5)$$

At this point, the measured energy dissipation for CSF E^{diss} (see Table 6.2) is used in Eq. (6.5) so that the product ρd can be estimated as follow:

$$\rho d = 0.073 \quad (6.6)$$

If a friction coefficient $\rho = 0.6$ is assumed, a value for the crack density d inside the CSF specimen can be evaluated as

$$d = 0.12 \quad (6.7)$$

As briefly said before, the crack density is a dimensionless parameter defined as

$$d = Na^3 \quad (6.8)$$

where N is the number of cracks per unit volume and a is the average radius of the cracks inside the unit volume itself. Using the same procedure for all the other specimens the product ρd can be estimated for each material and the resulting values are shown in Table 6.5. Considering the product ρd relative to the unmodified concrete as a reference quantity, the percentage change of the product ρd itself due to the addition of filler can be calculated and it is shown in Table 6.6

Specimen	ρd
CSF	0.074
CB3	0.072
CB7	0.066
CB0	0.078
CG3	0.079
CG7	0.083
CG0	0.071
CV3	0.071
CV7	0.064
CV0	0.107
CF3	0.059
CF7	0.062
CF0	0.087

Table 6.5: Estimated values for the product of the friction coefficient and the crack density

Specimen	% change of ρd
CSF	reference
CB3	-2.7
CB7	-10.2
CB0	+5.7
CG3	+6.6
CG7	+12.9
CG0	-3.4
CV3	-3.3
CV7	-12.4
CV0	+46.0
CF3	-19.4
CF7	-16.4
CF0	+18.2

Table 6.6: Estimated values for the product of the friction coefficient and the crack density

The two quantities ρ and d can not be separately estimated from the theory since they both appear on the right side of Eq. (6.1). In order to estimate the crack density d , a precise set of measures should then be prepared. In any case, a qualitative distribution of the crack density d can still be deduced from a set of experiments previously run by order of the Università di Roma "La Sapienza" at the "Istituto Sperimentale per la Meccanizzazione Agricola" (ISMA) in Rome. A set of specimens, equal to that one tested at Virginia Tech, was heated and the cooling off process was then monitored in order to make a qualitative estimate of the void density d of the matrix for each specimen. More particularly, each specimen was put in an oven at 150°C for 30 minutes; and the cooling off process was then observed by mean of a thermic camera. The thermal camera used is a very modern device which is able to detect the infrared radiation coming from a hot body and to transform this radiation into an apparent temperature. In this thesis, the results coming from the thermic analysis will be used just as a tool which can help in the interpretation of the results coming form the cyclic tests run at Virginia Tech. In particular, some graphics deriving from the thermic analysis performed in Rome can be considered helpful for the following considerations. These graphics shown in Fig. 6.3, 6.4, 6.5 and 6.6 show how the difference of temperature ΔT between the center and the external side of the specimen changes with time (the time $t = 0$ corresponds to the instant at which the specimen is removed from the oven). It can be easily understood that if a specimen has an high difference in temperature ΔT between its center and its external side at a given instant $\bar{t} > 0$, it means that the cooling off process is quick, while if ΔT is low at the same instant \bar{t} it means that the specimen take a longer time to cool off. Therefore, the higher is the curve in figures 6.3, 6.4,

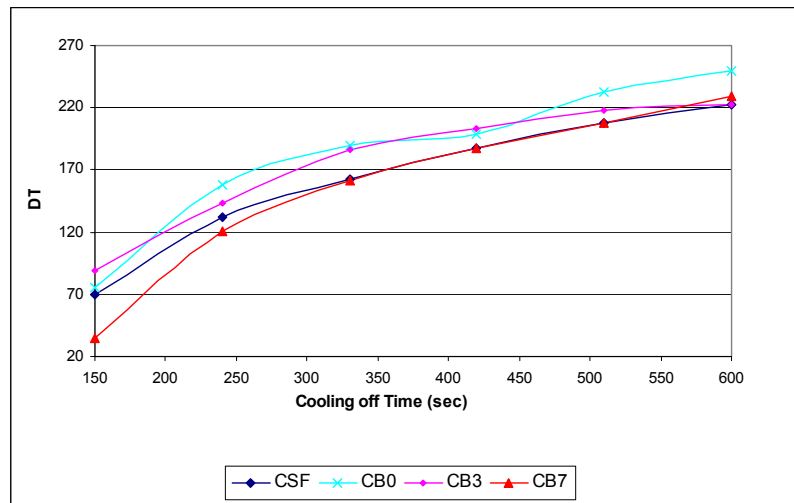


Figure 6.3: Cooling off behavior for CB specimens. Data from thermic tests run at the ISMA of Rome by order of "La Sapienza"

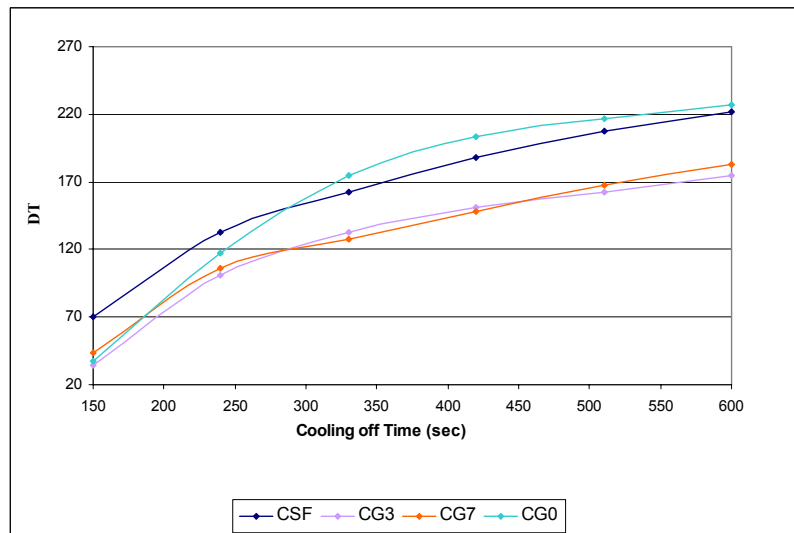


Figure 6.4: Cooling off behavior for CG specimens. Data from thermic tests run at the ISMA of Rome by order of "La Sapienza"

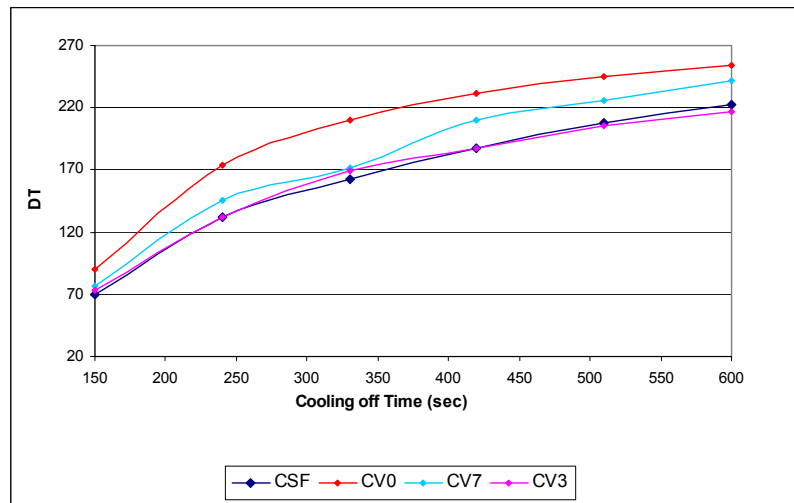


Figure 6.5: Cooling off behavior for CV specimens. Data from thermic tests run at the ISMA of Rome by order of "La Sapienza"

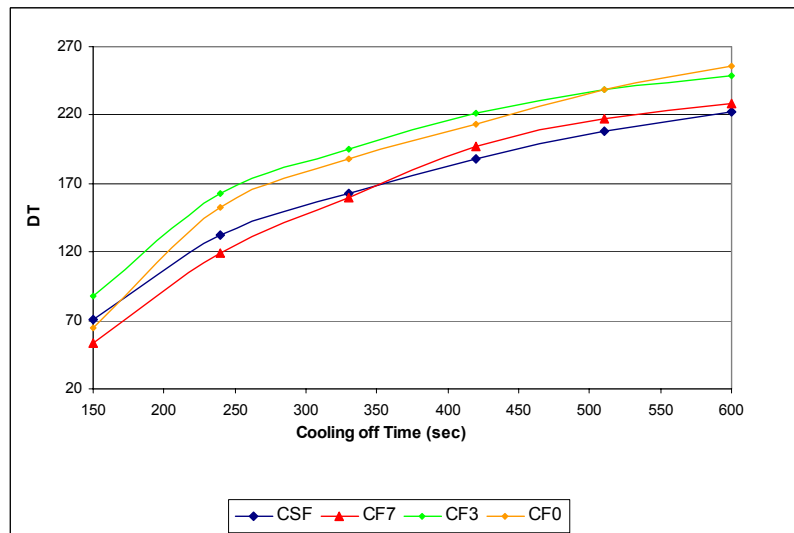


Figure 6.6: Cooling off behavior for CF specimens. Data from thermic tests run at the ISMA of Rome by order of "La Sapienza"

Specimen	d
CSF	d_{CSF}
CB3	$\leq d_{CSF}$
CB7	$> d_{CSF}$
CB0	$> d_{CSF}$
CG3	$< d_{CSF}$
CG7	$< d_{CSF}$
CG0	$\geq d_{CSF}$
CV3	$\simeq d_{CSF}$
CV7	$> d_{CSF}$
CV0	$\gg d_{CSF}$
CF3	$> d_{CSF}$
CF7	$< d_{CSF}$
CF0	$\gg d_{CSF}$

Table 6.7: Crack density values for the various fillers and percentages of replacement relative to the CSF crack density d_{CSF}

6.5 and 6.6, the quicker is the cooling off process. Moreover, it is also easy to understand that the higher is the slope of the curves shown in these graphics, the quicker the cooling off process is. At this point, if d_{CSF} is the crack density of the unmodified concrete it can be assumed, on the basis of the thermal analysis, if a given filler with a certain percentage of replacement increases or decreases the crack density of concrete (see Table 6.7). It must be noticed that the values of the crack density shown in table 6.7 have been estimated on the basis of the following assumption:

- *A specimen which presents a slower cooling off process than CSF has a lower crack density since the heat can not easily pass through a compact matrix. On the contrary, if a specimen presents a faster cooling off process, it will be assumed that it has a higher crack density compared to CSF.*

It is intuitive that this assumption can be considered sensible, even if there can exist some cases in which the assumption itself does not hold. In particular, for the CF7

specimen it can be noted that there is a period of ~ 340 seconds during which the specimen cools off more slowly than the CSF and after 340 seconds it cools off much quicker. This phenomenon can be explained assuming that the CF7 crack density is lower than the CSF one, and that the CF7 cracks are bigger than the CSF ones; this is in fact the hypothesis that will be used in the remainder of the thesis. At this point the product ρd calculated before (see Table 6.5) can be interpreted keeping in mind that we have some qualitative information both on the crack density d (from the thermic tests) and on the friction coefficient ρ (from the physical properties of the fillers see Table 3.1). First of all, as it can be immediately noticed from Table 6.5 the value of the product ρd has a very high value for the CV0 specimen. In this case, in fact, the product ρd seems to be well higher than the other cases. This is a very interesting result because it is an experimental proof of the validity of the frictional theory presented before. In fact, in the CV0 specimen a great quantity (10% in weight) of filler has been put in the cement paste; the filler used presents a smooth film on its surface so that a friction coefficient ρ lower than the CSF ρ is expected, at least for small percentages of replacement. In this case, in order to have a high product ρd like the one shown in Table 6.5 the crack density d must be very relevant. This is in fact the case as can be seen from the thermic experiments summarized in Table 6.7. Then, it can be stated that the experimental results are in good agreement with the frictional theory presented above. An experimental evidence of the increased value of the crack density for the CV0 specimen, can be found in the fact that the CV0 specimens both presented a macroscopic cracking phenomenon when subjected to the early cycles of the test, as can be seen from the photo shown in Fig. (6.7). The macroscopic cracking observed for the CV0 specimen



Figure 6.7: Macroscopic cracking for a CV0 specimen after few loading cycles

after the very early cycles indicates that the crack density in the material was very high, which is in good agreement with the theoretical prediction presented above. At this point, considering that we know whether the crack density d is higher or lower than the CSF one (see Tab. 6.7), and since we know the product ρd for each specimen (see Tab. 6.6 and fig. 6.8), we can tell whether a given filler with a certain percentage of replacement increases or decreases the friction coefficient ρ between the two faces of each crack. In order to be clear, each specimen will be discussed separately from the others; all the considerations in the following are referred to data summarized in Tab. 6.6 and 6.7.

- **CB3.** The thermic analysis shows that the crack density d of a CB3 specimen is expected to be higher than the CSF one, while the frictional sliding theory together with the data collected from tests run at Virginia Tech show that the product ρd is

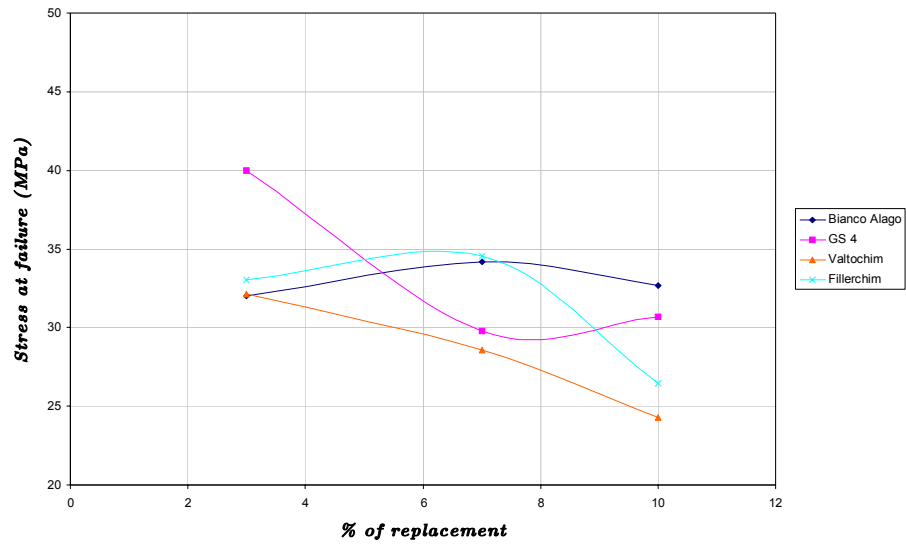


Figure 6.8: Variation of the product ρd with the percentage of replacement for each type of filler.

expected to slightly decrease compared to the CSF one. This means that the friction coefficient ρ must decrease more than d increases. This can be explained (see Table 3.1) because the Bianco Alago filler has round grains, even though it does not have a film on its surface, so that the grains slide on each other lowering the friction coefficient (see Fig. 6.9) compared to the CSF one. In other words

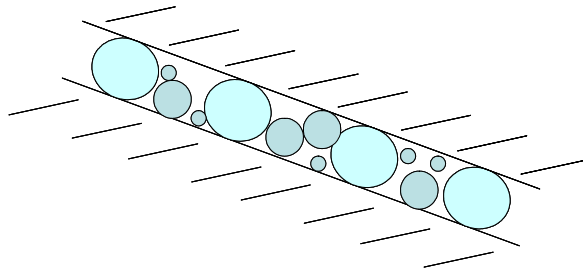


Figure 6.9: Frictional sliding of a crack in a CB3 specimen.

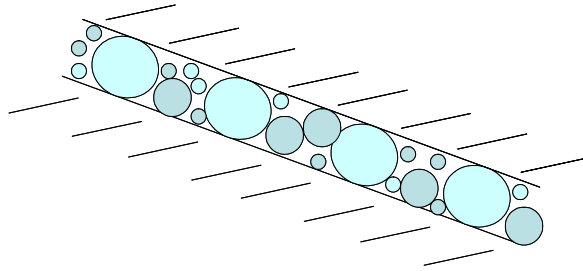


Figure 6.10: Frictional sliding of a crack in a CB7 specimen.

$$\rho_{CB3} < \rho_{CSF} \quad (6.9)$$

- **CB7.** The thermic analysis shows that the crack density d of a CB7 specimen is expected to be slightly lower than or equal to the CSF one, while the frictional sliding theory together with the data collected from tests run at Virginia Tech show that the product ρd is expected to decrease compared to the CSF one. This means that the friction coefficient ρ must decrease. This can be explained (see Table 3.1) because the Bianco Alago filler has round grains, even though it does not have a film on its surface, so that the grains slide on each other lowering the friction coefficient (see Fig. 6.10) compared to the CSF one. In other words

$$\rho_{CB7} < \rho_{CSF} \quad (6.10)$$

- **CB0.** The thermic analysis shows that the crack density d of a CB0 specimen is expected to be higher than the CSF one, while the frictional sliding theory together with the data collected from tests run at Virginia Tech show that the product ρd is expected to increase compared to the CSF one. This means that the friction coefficient ρ can be equal to or higher than the CSF one, or it can decrease less than d increases.

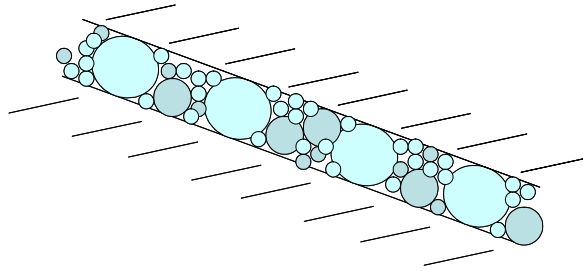


Figure 6.11: Frictional sliding of a crack in a CB0 specimen.

In this case we do not have a unique possibility for the value of ρ . In any case, we can imagine that the addition of filler still decreases the friction coefficient compared to the CSF one, but less than for the CB3 and CB7. Moreover ρ decreases less than the crack density d increases. This can be explained because when the percentage of replacement is too high, the filler "fills" the whole crack and the sliding process is not particularly improved (see Fig. 6.11).

- **CG3.** The thermic analysis shows that the crack density d of a CG3 specimen is expected to be lower than the CSF one, while the frictional sliding theory together with the data collected from tests run at Virginia Tech show that the product ρd is expected to increase compared to the CSF one. This means that the friction coefficient ρ must be higher than the CSF one. In other words

$$\rho_{CG3} > \rho_{CSF} \quad (6.11)$$

This can be explained (see Table 3.1) because the GS4 filler has irregular grains and it does not have a film on its surface, so that the grains can not easily slide on each other and the friction coefficient results to be higher than the CSF one (see Fig. 6.12).

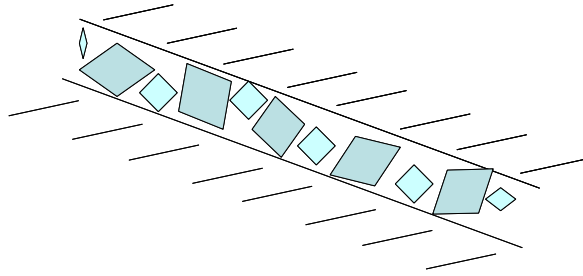


Figure 6.12: Frictional sliding of a crack in a CG3 specimen.

- **CG7.** The thermic analysis shows that the crack density d of a CG3 specimen is expected to be lower than the CSF one, while the frictional sliding theory together with the data collected from tests run at Virginia Tech show that the product ρd is expected to increase compared to the CSF one. This means that the friction coefficient ρ must be higher than the CSF one. In other words

$$\rho_{CG7} > \rho_{CSF} \quad (6.12)$$

Moreover, as it can be seen from Fig. 6.4 we can assume that

$$d_{CG7} \simeq d_{CG3} \quad (6.13)$$

and, as it is shown in tab. ,we also have

$$(\rho d)_{CG7} > (\rho d)_{CG3} \quad (6.14)$$

This means that the friction coefficient for CG7 increases more than the CG3 one, or in other words

$$\rho_{CG7} > \rho_{CG3} > \rho_{CSF} \quad (6.15)$$

where the inequalities (6.11) and (6.12) have also been used. The relationship between the various friction coefficients shown in (6.15) can be explained (see Table 3.1)

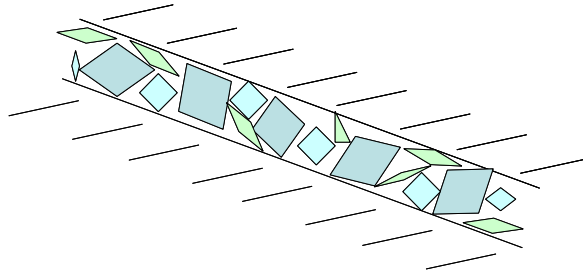


Figure 6.13: Frictional sliding of a crack in a CG7 specimen.

because the GS4 filler has irregular grains and it does not have a film on its surface, so that the grains can not easily slide on each other and the friction coefficient results to be higher than the CSF one (see Fig. 6.13). Moreover, the higher is the percentage of replacement the higher is the friction coefficient.

- **CG0.** The thermic analysis shows that the crack density d of a CG0 specimen is expected to be slightly higher than or equal to the CSF one (see also Fig. 6.4), while the frictional sliding theory together with the data collected from tests run at Virginia Tech show that the product ρd is expected to slightly decrease compared to the CSF one. This means that the friction coefficient ρ must be lower than the CSF one. In other words

$$\rho_{CG0} < \rho_{CSF} \quad (6.16)$$

The lower value of ρ can be explained only if we imagine that the GS4 filler has a critical percentage of replacement corresponding to which the friction coefficient changes from a value higher than the CSF one to a value lower than that. This can be true only if once the critical percentage of replacement is reached the grains start sliding on each other also if there is not a film on their surface. An explanation of

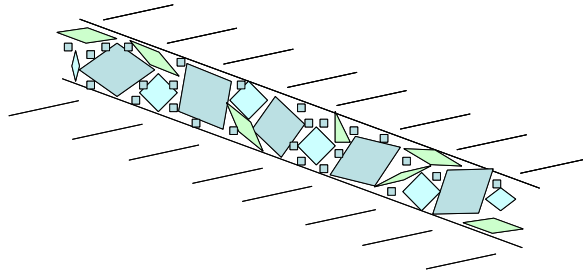


Figure 6.14: Frictional sliding of a crack in a CG0 specimen.

this phenomenon can be found in the fact that the smaller grains fill the gaps between the bigger ones and let them slide on each other lowering the friction coefficient (see Fig. 6.14). This does not exclude that another critical percentage of replacement, corresponding to which the friction coefficient rises again, can exist; this should be eventually verified preparing and testing specimens with percentages of replacement higher than 10%.

- **CV3.** The thermic analysis shows that the crack density d of a CV3 specimen is expected to be almost equal to the CSF one, while the frictional sliding theory together with the data collected from tests run at Virginia Tech show that the product ρd is expected to slightly decrease compared to the CSF one. This means that the friction coefficient ρ must decrease. In other words

$$\rho_{CV3} < \rho_{CSF} \quad (6.17)$$

It can be easily explained because the grains of the Valtochim filler have a smooth film on their surface, so that it can be expected that the friction coefficient is lower than the CSF one, at least for small percentages of replacement (see Fig. 6.15). Moreover

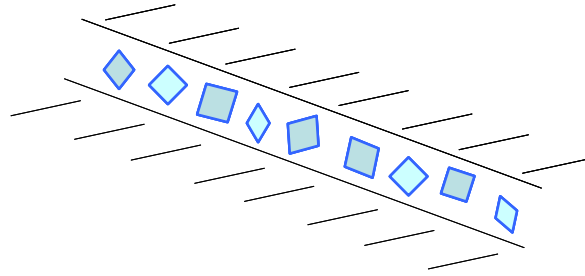


Figure 6.15: Frictional sliding of a crack in a CV3 and CF3 specimen.

the grain size for the Valtochim filler is $1-10\mu m$ so that the grains are small compared to the Bianco Alago and GS 4 ones (see Table 3.1) and an easier sliding process is then expected.

- **CV7.** The thermic analysis shows that the crack density d of a CV7 specimen is expected to increase with respect to the CSF one. On the other hand, the frictional sliding theory together with the data collected from tests run at Virginia Tech show that the product ρd is expected to decrease compared to the CSF one. This means that the friction coefficient ρ must decrease more than d increases. In other words

$$\rho_{CV7} < \rho_{CSF} \quad (6.18)$$

Moreover, since

$$(\rho d)_{CV7} < (\rho d)_{CV3} \quad (6.19)$$

and

$$d_{CV7} > d_{CV3} \quad (6.20)$$

then

$$\rho_{CV7} \ll \rho_{CV3} \quad (6.21)$$

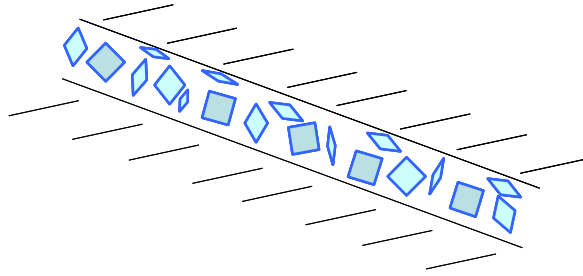


Figure 6.16: Frictional sliding of a crack in a CV7 and CF7 specimen.

This inequality together with (6.17) gives

$$\rho_{CV7} \ll \rho_{CV3} < \rho_{CSF} \quad (6.22)$$

so that it can be said that the friction coefficient for a CV7 specimen is very low compared to the CSF one. It can be explained thinking again that the grains surface of the Valtochim filler is smoothed by a film and assuming that a percentage of replacement of 7% is lower than an eventual critical value (see Fig. 6.16). The overall effect is then a lowering of the friction coefficient ρ .

- **CV0.** The thermic analysis shows that the crack density d of a CV0 specimen is expected to highly increase with respect to the CSF one. On the other hand, the frictional sliding theory together with the data collected from tests run at Virginia Tech show that the product ρd is expected to highly increase compared to the CSF one. This means that the friction coefficient ρ is undecidable. In fact it could theoretically increase as well or keep constant or slightly decrease resulting in any case in an increasing of the product ρd . On the basis of the physical properties of the Valtochim filler, we can imagine that the presence of the smooth film on the grain surface still

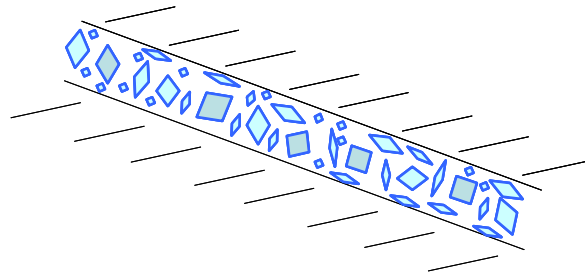


Figure 6.17: Frictional sliding of a crack in a CV0 and CF0 specimen.

lower the friction coefficient, even if the percentage of replacement is high. In any case, the friction coefficient of a CV0 specimen is expected to be closer to the CSF one than the CV3 and CV7 since the percentage of replacement is, in some way, approaching an eventual critical value (see Fig. 6.17)

- **CF3.** The thermic analysis shows that the crack density d of a CF3 specimen is expected to increase with respect to the CSF one. On the other hand, the frictional sliding theory together with the data collected from tests run at Virginia Tech show that the product ρd is expected to decrease compared to the CSF one. This means that the friction coefficient ρ must decrease more than d increases. In other words

$$\rho_{CF3} < \rho_{CSF} \quad (6.23)$$

It can be easily explained because the grains of the Fillerchim filler have a smooth film on their surface, so that it can be expected that the friction coefficient is lower than the CSF one, at least for small percentages of replacement (see Fig. 6.15). Moreover the grain size for the Fillerchim filler is $1-20\mu m$ so that the grains are small compared to the Bianco Alago and GS 4 ones (see Table 3.1) and an easier sliding process is

then expected.

- **CF7.** The thermic analysis shows that the crack density d of a CF7 specimen is expected to be lower than the CSF one. On the other hand, the frictional sliding theory together with the data collected from tests run at Virginia Tech show that the product ρd is expected to decrease compared to the CSF one. This means that the friction coefficient ρ can decrease, keep constant or slightly decrease compared to the CSF one.
- **CF0.** The thermic analysis shows that the crack density d of a CF0 specimen is expected to increase with respect to the CSF one. On the other hand, the frictional sliding theory together with the data collected from tests run at Virginia Tech show that the product ρd is expected to increase compared to the CSF one. This means that the friction coefficient ρ is undecidable. In fact it could theoretically increase as well or keep constant or slightly decrease resulting in any case in an increasing of the product ρd . We will assume that ρ_{CF0} is slightly lower than or almost equal to ρ_{CSF} . This can be explained assuming that the quantity of filler added is so relevant that grains can not easily slide on each other (see Fig. 6.17)

The qualitative analysis made above for all the different specimens can be considered fairly reliable. At this point on the basis of the previous considerations, some assumptions on the mechanical resistance of the different specimens can be made and they can then be validated by mean of the ramp tests run at Virginia Tech. These considerations are presented in the next section

6.3 Possible correlation between the product ρd and the mechanical properties of the concrete-like materials.

A possible correlation between the friction coefficient ρ , the crack density d and the mechanical resistance σ_f of the different specimens is now investigated. For the sake of simplicity, the different specimens will be analyzed separately in and all the considerations made on the basis of the value of the product ρd will then be compared with the actual results obtained from the ramp tests run at Virginia Tech and summarized in Table 5.2 and in Fig. 6.18. From an intuitive point of view, it is easy to understand that if the friction coefficient between the two faces of each crack increases, σ_f is expected to increase as well because the sliding motion of the faces themselves is in some way impeded. On the other hand, if the crack density is increased with respect to the plain concrete, one can imagine that σ_f decreases.

- **CB3.** As it has been previously observed we have

$$d_{CB3} > d_{CSF} \quad (6.24)$$

and

$$\rho_{CB3} < \rho_{CSF} \quad (6.25)$$

so that for both (6.24) and (6.25) the expected result is

$$\sigma_f^{CB3} < \sigma_f^{CSF} \quad (6.26)$$

which is in fact the case (see Fig. 6.18). In this case the frictional sliding theory and the experimental evidence are in good agreement.

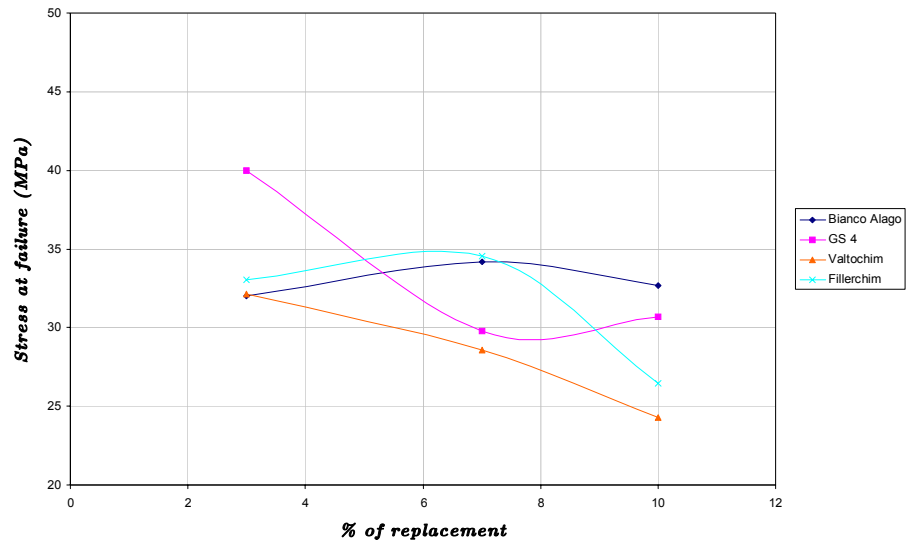


Figure 6.18: Stresses at failure for all the percentages of replacement of the various fillers. Data from tests run at Virginia Tech.

- **CB7.** As it has been previously observed we have

$$d_{CB7} \simeq d_{CSF} \quad (6.27)$$

and

$$\rho_{CB7} < \rho_{CSF} \quad (6.28)$$

so that for both (6.27) and (6.28) the expected result is

$$\sigma_f^{CB7} < \sigma_f^{CSF} \quad (6.29)$$

As can be seen from Fig. 6.18 this is in fact the case. The fact that $\sigma_f^{CB7} > \sigma_f^{CB3}$ can be due to the fact that for a percentage of replacement of 7% the crack density seems to be reduced.

- **CB0.** As it has been previously observed we have

$$d_{CB0} \gg d_{CSF} \quad (6.30)$$

and

$$\rho_{CB0} \leq \rho_{CSF} \quad (6.31)$$

We can see from (6.30) that the crack density of the CB0 specimen is expected to be very high compared to the CSF one. At the same time the friction coefficient is not expected to change much, so that the expected result is

$$\sigma_f^{CB0} < \sigma_f^{CSF} \quad (6.32)$$

which is in fact the case (see Fig. 6.18). In this case the frictional sliding theory and the experimental evidence are in good agreement.

- **CG3.** As it has been previously observed we have

$$d_{CG3} < d_{CSF} \quad (6.33)$$

and

$$\rho_{CG3} > \rho_{CSF} \quad (6.34)$$

so that for both (6.33) and (6.34) the expected result is

$$\sigma_f^{CG3} > \sigma_f^{CSF} \quad (6.35)$$

which is in perfect agreement with the observed results (see fig. 6.18). So, also in this case the frictional sliding theory and the experimental evidence are in good agreement.

From an engineering point of view, the improved mechanical resistance for the CG3

specimen is the most interesting result, as can be easily intuited and as it will be shown in the conclusions of this thesis.

- **CG7.** As it has previously observed we have

$$d_{CG7} < d_{CSF} \quad (6.36)$$

and

$$\rho_{CG7} > \rho_{CSF} \quad (6.37)$$

so that for both (6.36) and (6.37) the expected result is

$$\sigma_f^{CG7} > \sigma_f^{CSF} \quad (6.38)$$

The result that actually turns out from the ramp failure tests shows an opposite behavior compared to the inequality (6.38), in other words the actual case gives (see Fig. 6.18)

$$\sigma_f^{CG7} < \sigma_f^{CSF} \quad (6.39)$$

In this case the frictional sliding theory and the experimental results can definitely not be considered in agreement. If we consider that the assumptions on the crack density deriving from the thermic analysis (see ((6.36))) are reliable, we must tell that the frictional sliding theory does not predict the real behavior of the material in this case. This can be due perhaps to the fact that one of the hypothesis used to obtain the simplified expression (6.1) does not hold for the CG7 specimen. It is for this reason that further experiments are needed in order to clear this incongruence.

- **CG0.** In this case it has been seen that

$$d_{CG0} > d_{CSF} \quad (6.40)$$

and

$$\rho_{CG0} < \rho_{CSF} \quad (6.41)$$

so that for both (6.40) and (6.41) the expected result is

$$\sigma_f^{CG0} < \sigma_f^{CSF} \quad (6.42)$$

which is in fact the case (see Fig. 6.18). Also in this case, the experimental results are in good agreement with the frictional sliding theory.

- **CV3.** As far as the CV3 specimen is concerned, it has been shown that

$$d_{CV3} \simeq d_{CSF} \quad (6.43)$$

and

$$\rho_{CV3} < \rho_{CSF} \quad (6.44)$$

so that the following inequality for the stress at failure is expected to hold

$$\sigma_f^{CV3} < \sigma_f^{CSF} \quad (6.45)$$

which is in fact the case (see Fig. 6.18).

- **CV7.** For the CV7 specimen we saw that

$$d_{CV7} > d_{CSF} \quad (6.46)$$

and

$$\rho_{CV7} \ll \rho_{CV3} < \rho_{CSF} \quad (6.47)$$

so that the stress at failure is expected to be such that

$$\sigma_f^{CV7} < \sigma_f^{CV3} < \sigma_f^{CSF} \quad (6.48)$$

which is in fact the case (see Fig. 6.18).

- **CV0.** It has been observed that

$$d_{CV0} \gg d_{CSF} \quad (6.49)$$

the crack density for the CV0 specimen is so high that a macroscopic cracking phenomenon was observed after the first cycles of the experiment. It is for this reason that, no matter which is the value of the friction coefficient, the mechanical strength is expected to be well below the CSF value, i.e.

$$\sigma_f^{CV0} < \sigma_f^{CSF} \quad (6.50)$$

which is actually true (see Fig. 6.18).

- **CF3.** It has been seen that

$$d_{CF3} > d_{CSF} \quad (6.51)$$

and

$$\rho_{CF3} < \rho_{CSF} \quad (6.52)$$

so that the following result is expected

$$\sigma_f^{CF3} < \sigma_f^{CSF} \quad (6.53)$$

which is in fact the case (see Fig. 6.18).

- **CF7.** For the CF7 specimen we saw that

$$d_{CF7} < d_{CSF} \quad (6.54)$$

and that the friction coefficient variation is undecidable. From the experimental results, we can see that

$$\sigma_f^{CF7} \simeq \sigma_f^{CSF} \quad (6.55)$$

so that we can assume that the friction coefficient decrease as well compared to the CSF one in such a way that the decrease in d_{CF7} balances the decrease in ρ_{CF7} so that (6.55) can hold.

- **CF0.** As far as the CF0 is concerned, it has been previously seen that

$$d_{CF0} \gg d_{CSF} \quad (6.56)$$

so that the mechanical properties of the specimen are expected to be worse than the CSF ones, or

$$\sigma_f^{CF0} < \sigma_f^{CSF} \quad (6.57)$$

which is in fact the case (see Fig. 6.18).

The qualitative analysis shown up to now can be summarized using the bar charts below (see Fig. 6.19, 6.20, 6.21, 6.22 and 6.23). As already observed before, it can be easily seen from Fig. 6.23 and 6.24 that the predicted and the actual results are in good agreement, except for the CG7 specimen. This incongruence is probably due by the fact that one of the hypothesis used in the micro-macro identification does not hold for the CG7 specimen case. A more accurate analysis is then needed to study the CG7 specimen behavior.

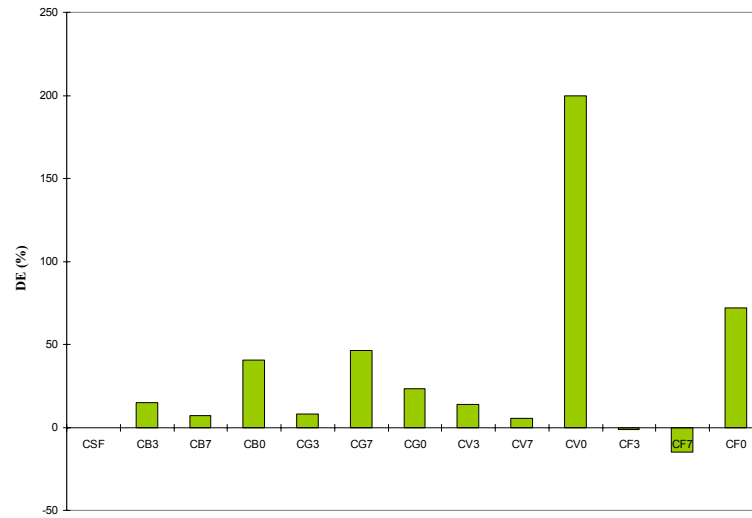


Figure 6.19: Percent variation of the average energy dissipation of each specimen compared to the CSF energy variation. Data comes from cyclic tests run at Virginia Tech.

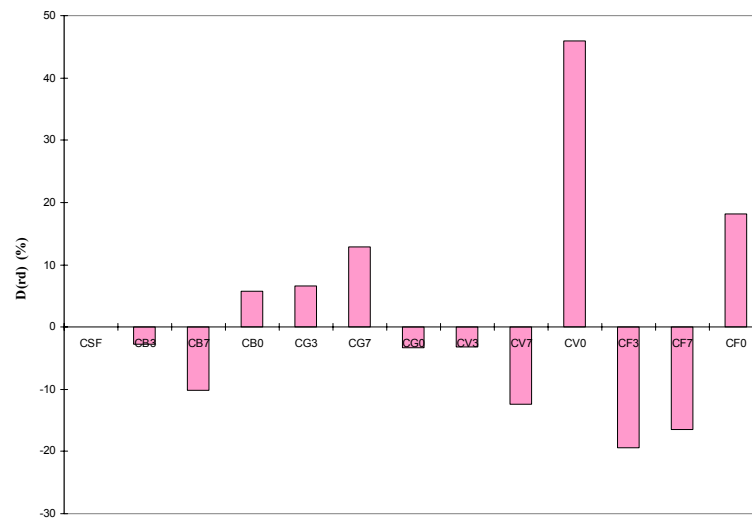


Figure 6.20: Percent variation of the product ρd as calculated from the coupling between the micro-macro frictional theory and the energy dissipation measures from cyclic tests.

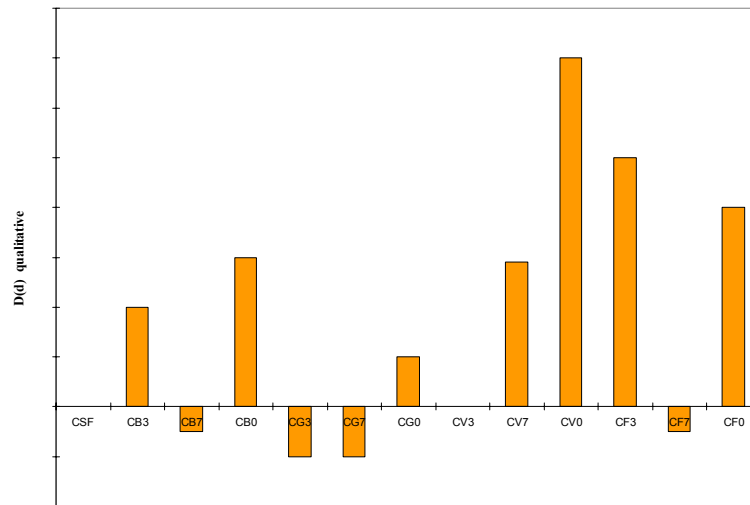


Figure 6.21: Qualitative variation of the crack density d with respect to the CSF one. Data from thermic tests run at Università di Roma "La Sapienza".

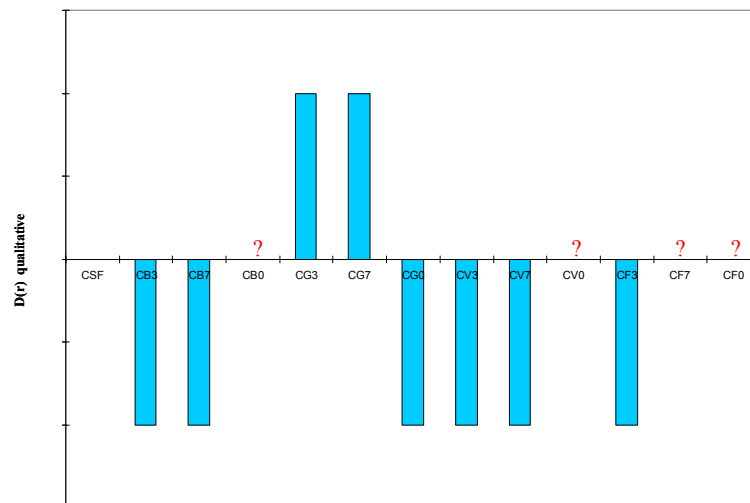


Figure 6.22: Qualitative variation of the friction coefficient ρ for the various specimens with respect to the CSF one. This qualitative estimate has been made on the basis of the calculated values of the product ρd (see Fig. 6.20) and of the predicted crack density estimated from thermic analysis (see Fig. 6.21)

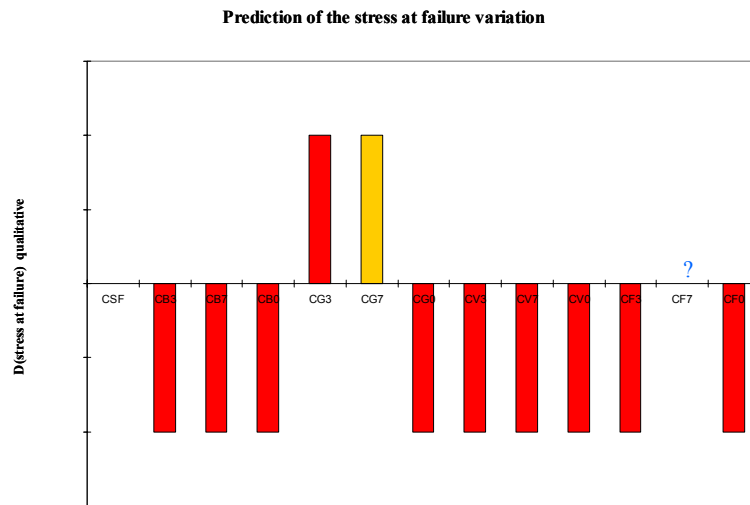


Figure 6.23: Qualitative prediction of the stress at failure variation on the basis of the qualitative variations of ρ and d given in Fig. 6.21 and 6.22.

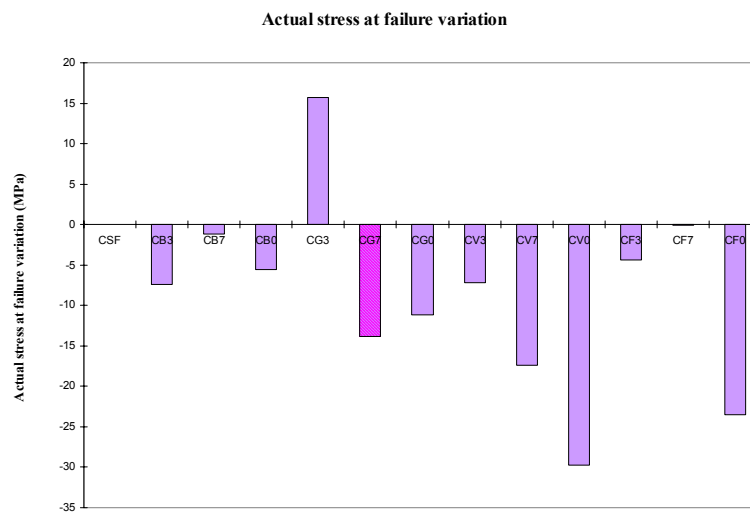


Figure 6.24: Actual stress at failure variation from measures deriving from ramp failure tests run at Virginia Tech.

Chapter 7

Conclusions and Recommendations

Concrete has a very old and interesting story. More than 2000 years ago, an ancient Roman writer, Vitruvio, showed in his book, "De Architectura", how it was used for building construction during the Roman Empire. The way the ancient Romans prepared and used concrete can be of course considered primitive compared to the modern technologies, but the fact that this material is being used for such a long time indicates that its performance has been considered, for two thousand years, irreplaceable. Nowadays, more than 90% of European civil constructions are concrete-based structures, and this percentage clearly indicates the importance of this material for engineering. The European Community has a precise set of rules for concrete that engineers have to respect every time they design a concrete-based structure. More particularly, concrete must have precise mechanical properties in order to be used for any type of construction. Any time a new structure is being built, a set of specimens of the concrete used must be sent to an authorized laboratory which performs a series of tests, establishing if that concrete has acceptable mechanical properties

or not. There are very few laboratories which can do this kind of test, and all of them must have a Government authorization which states that the staff is highly qualified and able to run concrete testing. In order to have an idea of the concrete business dimensions in Europe, we can tell that one half of the non-state income (6 millions of Euros per year) for the department of "Structural and Geotechnical Engineering" at the University of Rome, "La Sapienza" comes from concrete testing. It is for these reasons that in the last decades many scientists focused their attention on improving the mechanical properties of concrete. It is in fact clear, for example, that a material with higher strength and the same specific weight of the common concrete would be very useful in Civil Engineering applications. In this case, in fact, a smaller quantity of concrete would be needed to build the same structure maintaining the same safety factor. On the basis of this example, it becomes clear that another parameter has to be considered: the cost of the new material. In fact, if the new material has a higher strength and the same specific weight as the common concrete, this is not useful if its cost is too high compared to the common concrete. Thus, we can tell that there are 3 parameters that must be taken into account when designing a new material which can replace concrete:

- Mechanical Properties (stress at failure, elastic modulus, etc.).
- Physical properties (specific weight, etc.).
- Cost.

The set of specimens used for the tests presented in this thesis has been prepared substituting a certain percentage in weight of cement powder with the same percentage in

weight of one of the fillers shown in Table 3.1. These fillers have been chosen for 2 different reasons, which are listed below:

1. Their *physical properties* (e.g., size, roughness of the grain surface, etc.) which were expected, as explained before, to change the friction coefficient (and then the mechanical properties) between the two faces of the cracks inside the cement matrix.
2. Their *cost*.

As it has been seen in the Analysis of Results section, only one specimen, the CG3, has been found to have a higher strength than the normal concrete, but this result is significant if we note that the specific weight and the cost of the new material are almost the same as for the common concrete. Moreover, the stress at failure for the CG3 was found to be more than 15% higher than for the common concrete. This is exactly the case we were considering before; the CG3 material could be used to build a structure with a smaller quantity of material, while maintaining the same safety factor and the same cost. It is for this reason that further experiments should be run, focusing the attention on the CG3 specimen. In fact, there were only 2 CG3 specimens tested at Virginia Tech and 2 tested at "La Sapienza"; all of them showed an improved mechanical resistance. Hence a larger number of CG3 specimens should be prepared and tested in order to perform a statistical analysis of the results. Moreover, specimens with percentages of replacement of GS4 filler slightly lower (and higher) than 3% should be prepared, in order to see if there is an optimal percentage of replacement corresponding to which there is an absolute maximum for the stress at failure. It has also been seen that the analysis of results performed in the previous section was simply a *qualitative* analysis. In fact, once the product ρd was

calculated for each specimen, there was no possibility to find a precise value for each term separately, and only a qualitative estimate of the crack density d (and subsequently of the friction coefficient ρ) was possible on the basis of a thermic analysis previously run at "La Sapienza". In order to find a precise numerical value for d a set of measures of the crack density (*quantitative analysis*) should be run with microscopes or some other device. In this way, once d would be known the friction coefficient could be exactly estimated by means of Eq. (6.5) and more accurate predictions could be made. Moreover, it has been seen before that the cyclic experiments run at Virginia Tech have been prepared in order to assure that the damage (crack density d) did not evolve during the cycling; this was done using a low stress range. This approach, limited to non-evolving damage situations is interesting and useful in order to predict the behavior of a concrete-based structure under a given set of external loads. This prediction is essential in all engineering situations, since, when designing a new structure, an engineer must be sure that the structure itself can sustain the applied external load without catastrophic failure. There are 3 types of external forces that must be taken into account in structures design

- *Fixed loads.* These loads are all the forces that act on the structure in every instant of its engineering life, such as the weight of the structure itself.
- *Variable loads.* These loads are represented by those forces which act on the structure periodically, such as the weight of people which are presumed to stay in the building or the weight of furnitures, etc.
- *Accidental loads.* These loads are of a very different type with respect to the first two ones; in fact, they are all those forces which can act on the structure, but that can not

be predicted in a precise way. These type of forces are taken in great consideration in Europe and must be always taken into account in engineering design. In this class of forces, in fact, are included the forces generated by *earthquakes*. The problem of earthquakes is very common in Europe, and specifically in Italy, where a set of technical rules have been prepared by the Italian Government and must be carefully respected by all engineers.

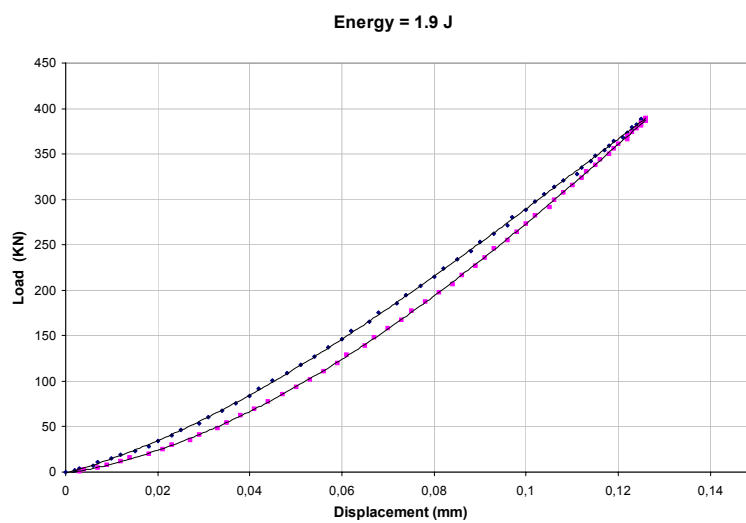
As far as the fixed load are concerned, they can be exactly predicted, and then they are easily taken into account in engineering calculations. Analogously, the variable loads can be safely estimated; in fact, the maximum possible load which can be reached in a given building is calculated and this load is used then in calculations. It is for this reason that, once the external load given by fixed and variable forces is known, a proper safety factor can be applied, and the response of the structure to those forces can be predicted. In this first step of the design process, the only information needed are the mechanical properties of the materials used (in our specific case of concrete) under constant loads. It is for this reason that non-evolving damage situations can be in this case considered in order to estimate the mechanical properties of concrete; in fact, damage-evolution situations for concrete are expected to happen when periodic (cyclic) loads of a certain intensity are applied to the material. On the basis of these considerations, it is clear that the set of experiments run at Virginia Tech, designed in such a way that the absence of damage evolution was assured, are essential for the prediction of concrete response to a set of fixed and variable external forces. These kind of experiments are then really useful to the first step of the design process. As already said, this first step of designing is essential, but

it is not sufficient to assure the safety of the structure. In fact, there are the accidental loads, such as the earthquakes, which cannot be predicted and which are cyclic forces of great intensity. These kind of forces are of course expected to generate damage-evolution processes in the cement matrix, so that the experiments considered in these thesis cannot be helpful in this case. It is for this reason that further experiments could be prepared with an higher stress range than the one used at Virginia Tech, which allow a certain damage evolution inside the cement matrix. In this case, the theory used in this thesis (see Eq. (2.23)) to predict the behavior of the material does not hold anymore and more accurate theories involving damage evolution should be used. A theoretical approach to frictional sliding phenomena with damage evolution processes has been recently presented by Pensée et al., 2002, even if there are not experimental validations of this theory.

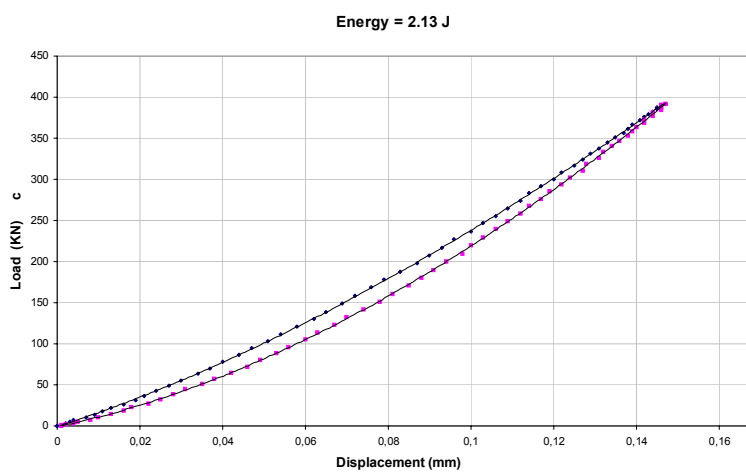
Appendix A

Energy dissipations

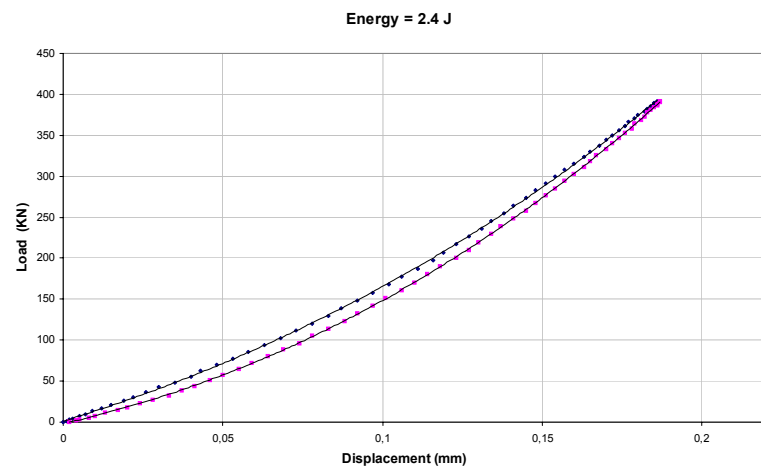
This appendix is a collection of all the graphics referring to the 50th cycle hysteresis loop. As already said before, the curves fitting the data points are all 3rd order polynomials. In each graphic is also reported the measured energy dissipation relative to the considered cycle, measured in Joules. It must be noticed that the zero load shown in each picture of this appendix corresponds to the minimum load applied (see Tab. 4.2), so that the values shown on the y axis actually correspond to the load range.



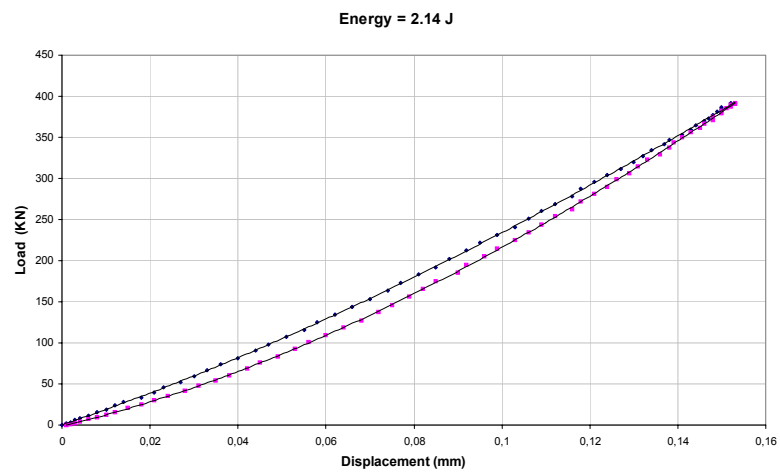
Hysteresis loop for the CSFA specimen



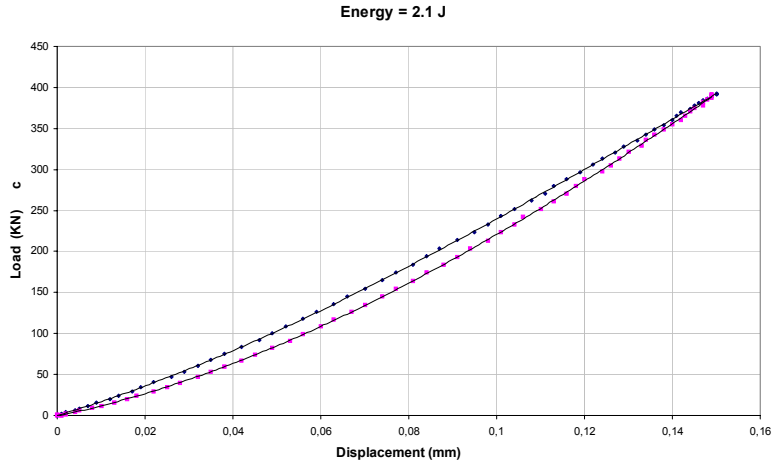
Hysteresis loop for the CSFB specimen



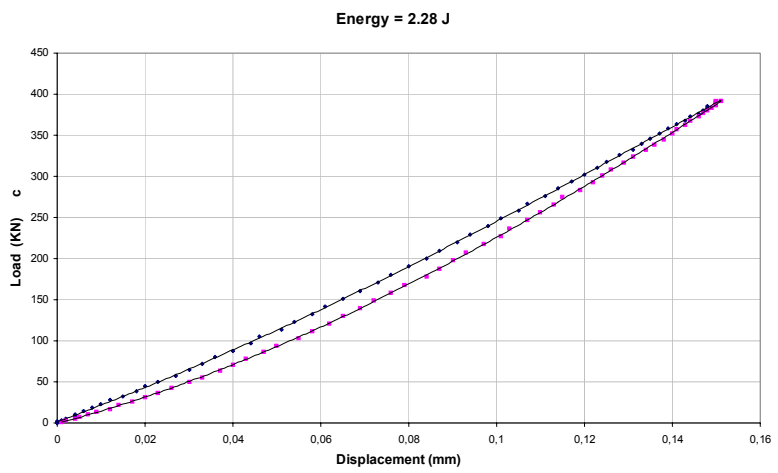
Hysteresis loop for the CB3A specimen



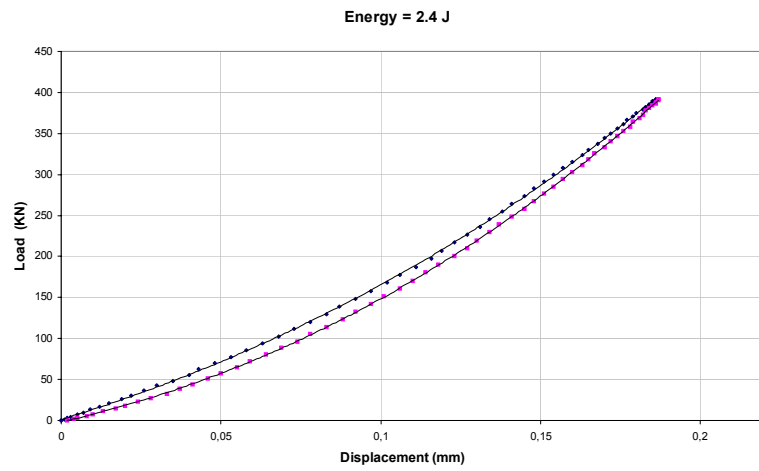
Hysteresis loop for the CB3B specimen



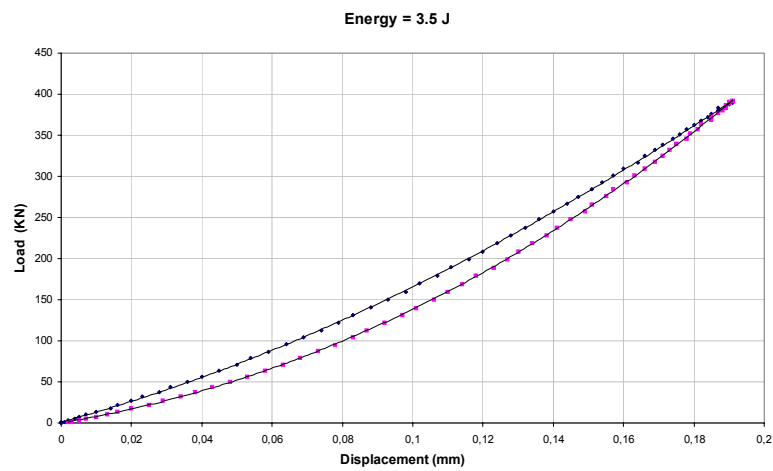
Hysteresis loop for the CB7A specimen



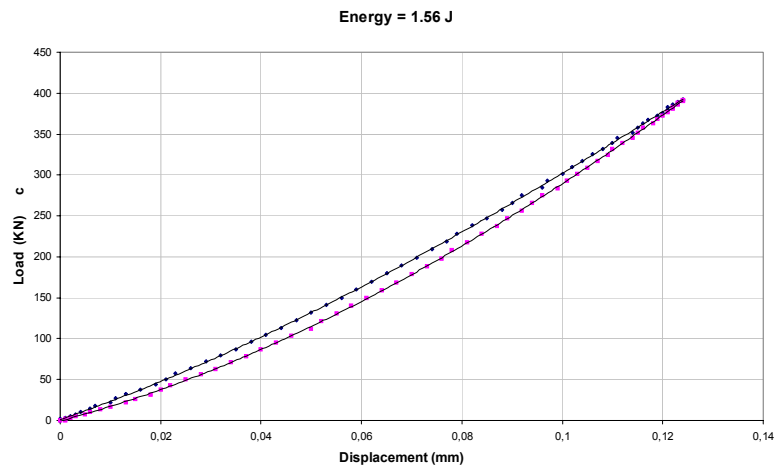
Hysteresis loop for the CB7B specimen



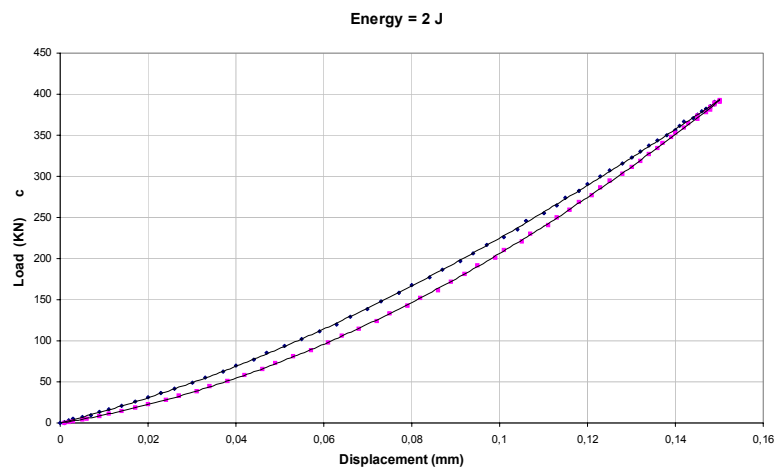
Hysteresis loop for the CB0A specimen



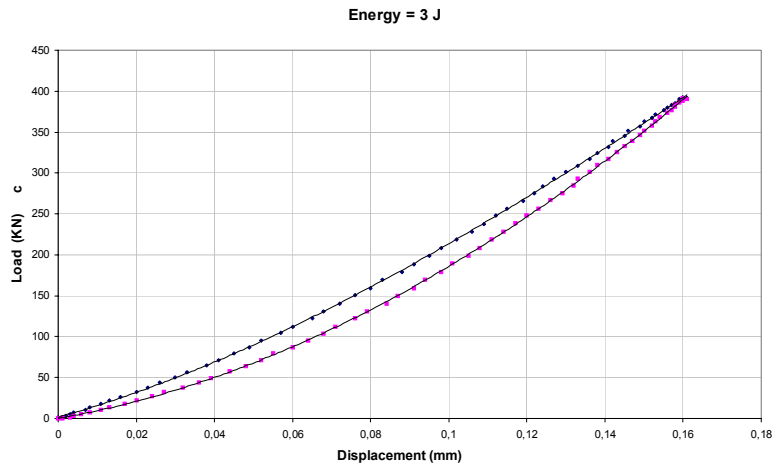
Hysteresis loop for the CB0B specimen



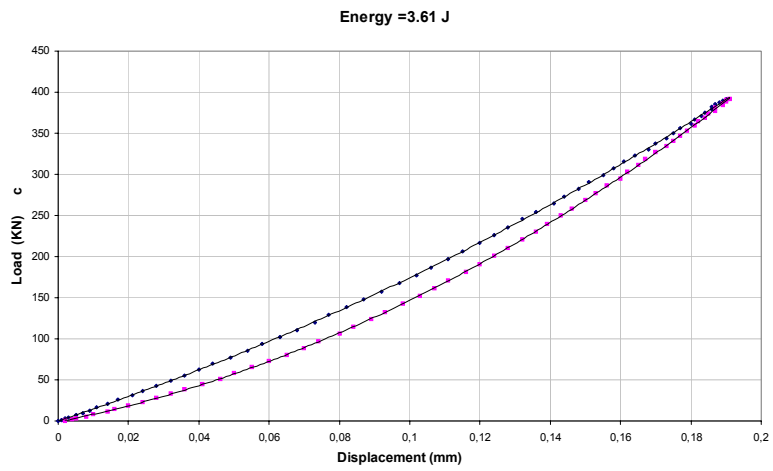
Hysteresis loop for the CG3A specimen



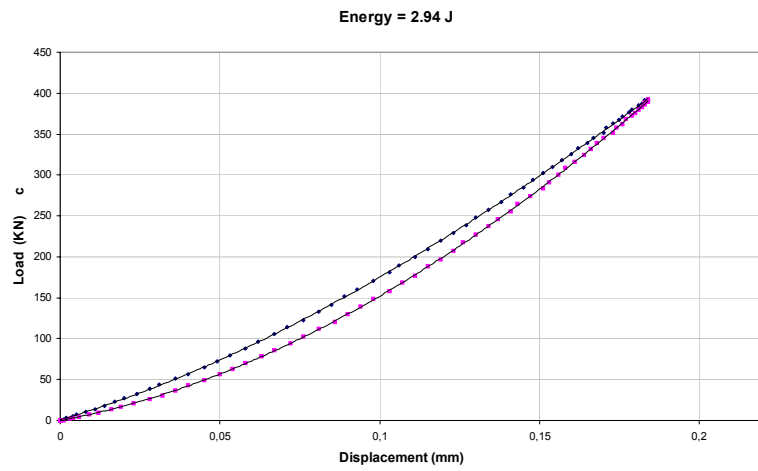
Hysteresis loop for the CG3B specimen



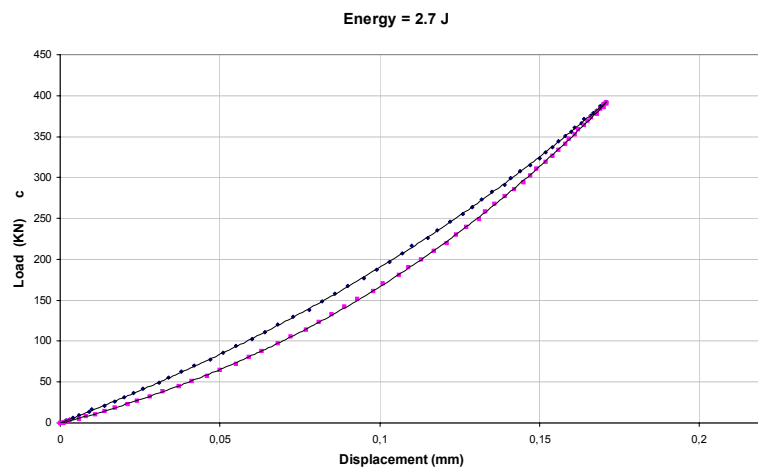
Hysteresis loop for the CG7A specimen



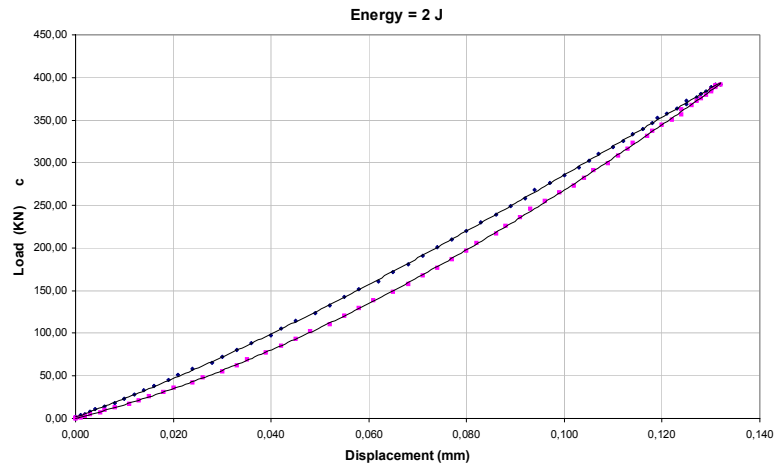
Hysteresis loop for the CG7B specimen



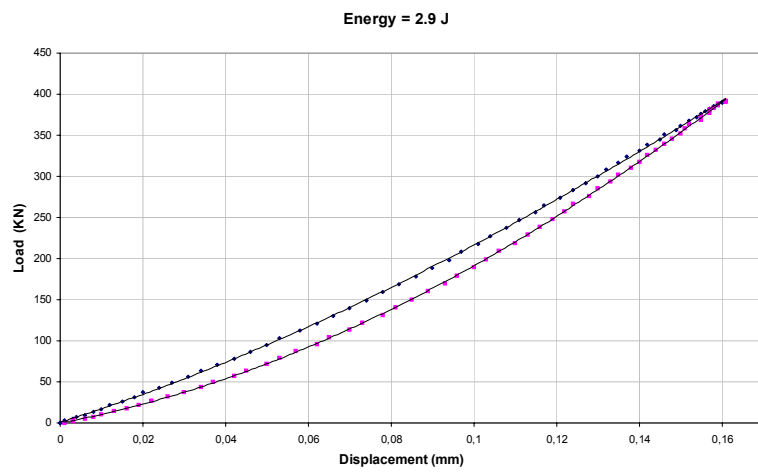
Hysteresis loop for the CG0A specimen



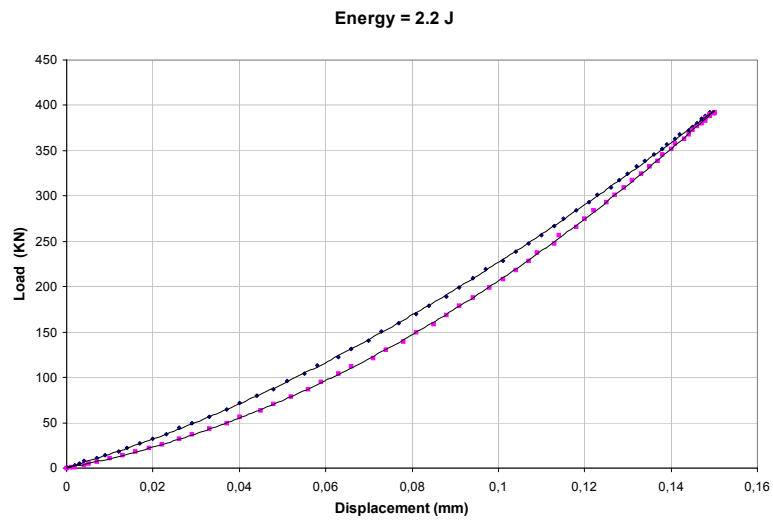
Hysteresis loop for the CG0B specimen



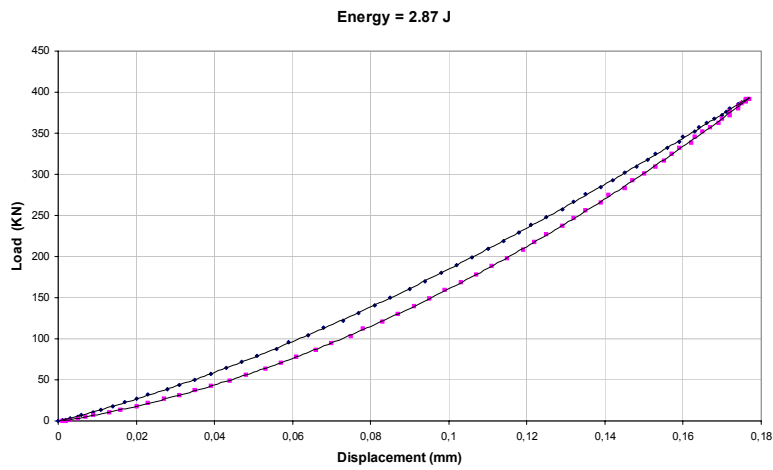
Hysteresis loop for the CV3A specimen



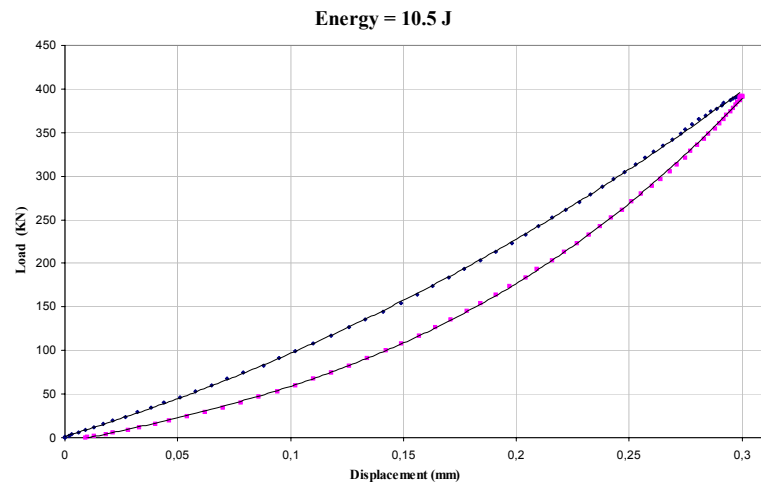
Hysteresis loop for the CV3B specimen



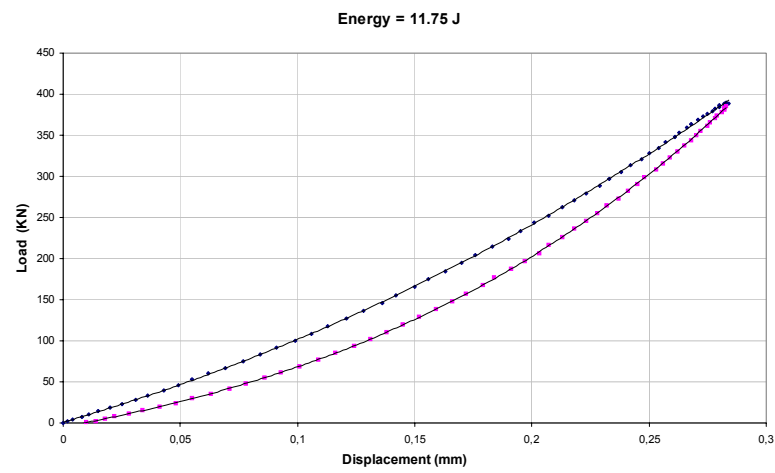
Hysteresis loop for the CV7A specimen



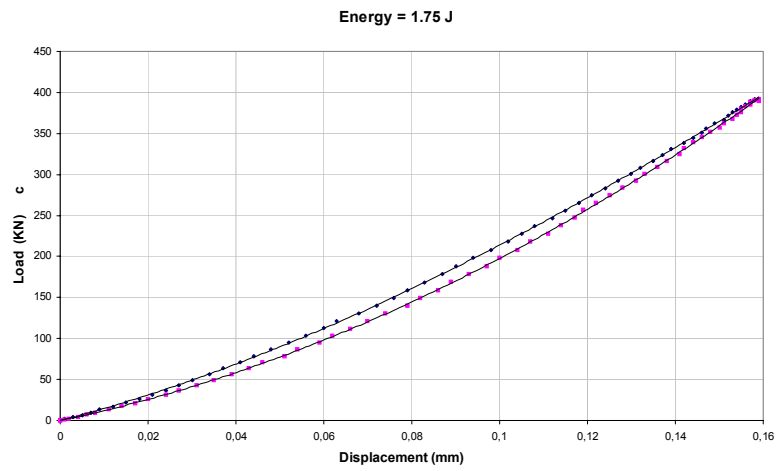
Hysteresis loop for the CV7B specimen



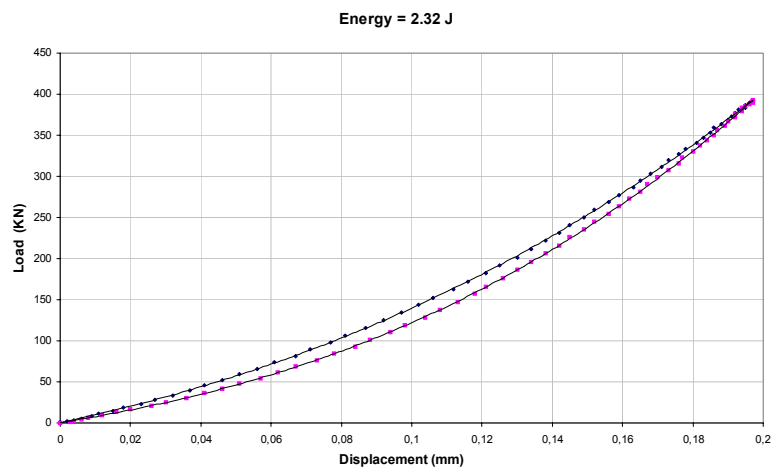
Hysteresis loop for the CV0A specimen



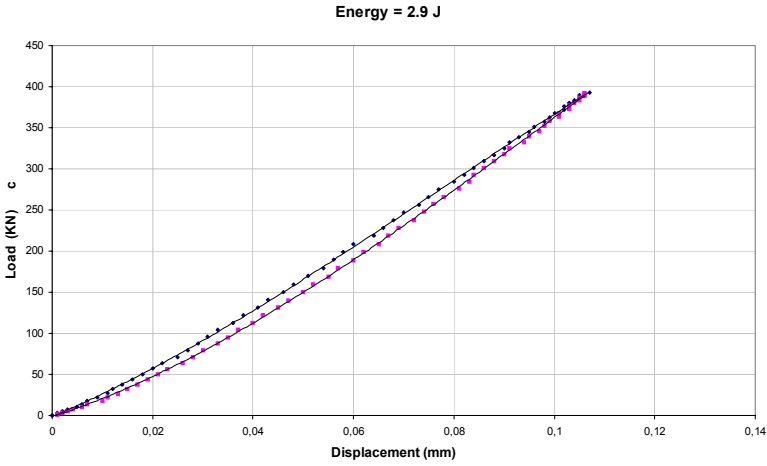
Hysteresis loop for the CV0B specimen



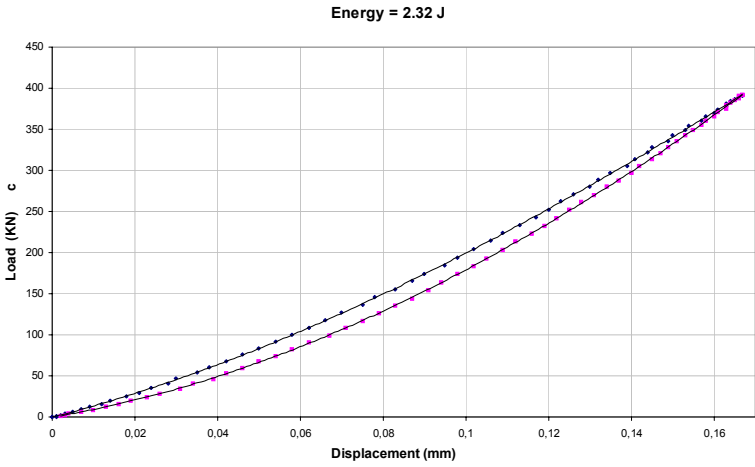
Hysteresis loop for the CF3A specimen



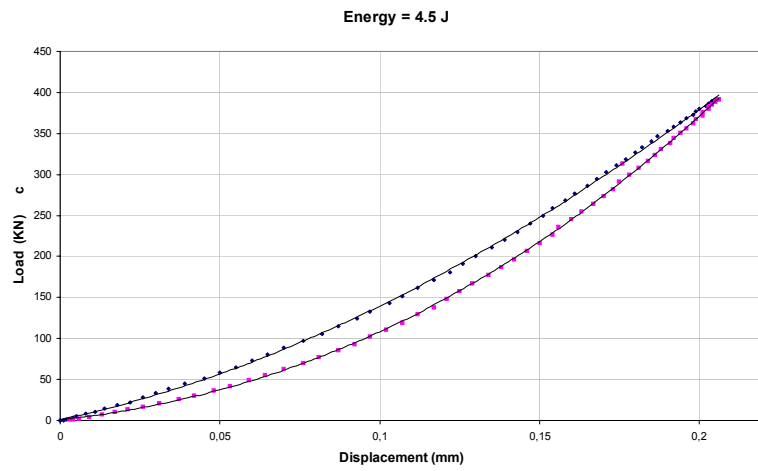
Hysteresis loop for the CF3B specimen



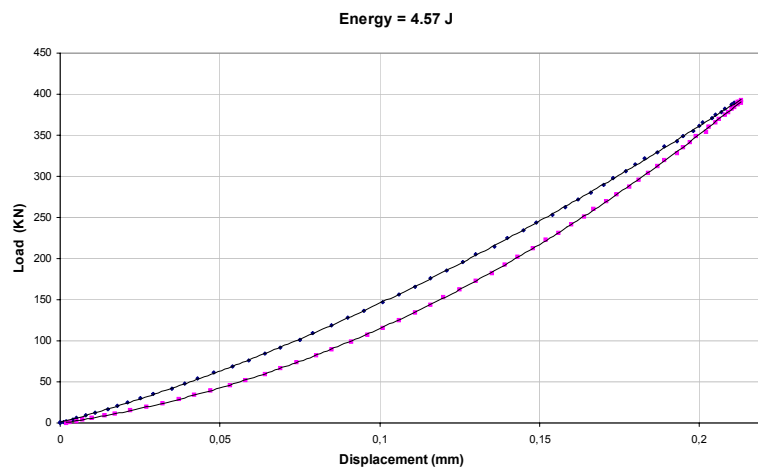
Hysteresis loop for the CF7A specimen



Hysteresis loop for the CF7B specimen



Hysteresis loop for the CF0A specimen



Hysteresis loop for the CF0B specimen

Bibliography

- [1] Pensée V., D. Kondo, L.Dormieux (2002); "Micromechanics of anisotropic damage in rocks and concrete: unilateral effects modeling and coupling with friction", 15th ASCEE Engineering Mechanics Conference, June 2-5 2002, Columbia University, NJ.
- [2] Pensée (2002); Contribution de la micromécanique à la modélisation tridimensionnelle de l'endommagement par mésolfissuration, PhD thesis.
- [3] Bennett E.W., (1980) "Fatigue of plain concrete in compression under varying sequences of two-level programme loading", *Int. J. Fatigue*, **2**(4), 171-175
- [4] Dowling N.E. (1999), *Mechanical Behavior of Materials*, Prentice Hall, N.J.
- [5] Kachanov M. (1981); "A microcrack model of rock inelasticity: frictional sliding on microcracks", *Mech. Mater.*, **1**, 19-27.
- [6] Andrieux S., Y. Bamberger, J.J. Marigo (1986); "Un modèle de matériau microfissuré pour les roches et les bétons", *J. of Mécanique Théorique et Appliquée*, **5**(3), 471-513.
- [7] Nemat-Nasser S., M. Obata (1988); "A microcrack model of dilatancy in brittle materials", *J. of Applied Mechanics*, **55**, 24-35.

- [8] Lee X., J.W. Ju (1991); "Micromechanical Damage Model for Brittle Solids: Compressive Loadings", *J. Engrg. Mech.* ASCE, **117**, 1515-1536.
- [9] Gambarotta L., S. Lagomarsino (1993), "A Microcrack Damage Model for Brittle Materials", *Int. J. Solids Structures*, **30**(2), 177-198.
- [10] Pensée V., D. Kondo, L.Dormieux (2002); "A Micromechanical Analysis of Anisotropic Damage in Brittle Materials", *J. Engrg. Mech.*